Synthesis, Characterization and Antibacterial Activity of Nano-Magnesium Nickel Oxide

By

Memoona Qammar

A dissertation submitted in partial fulfillment of the requirements for the

Degree of Master of Science in Chemistry

Supervised by

Dr. Zahida Malik

Department of Chemistry

School of Natural Sciences

National University of Sciences & Technology

Islamabad, Pakistan

2017

Praise is due to ALLAH whose worth cannot be described by speakers [Nahj-al-Balagha].

Acknowledgements

Dedicated to my Parents Kausar Batool & Qammar Abbas

Table of Contents

Contents

Abstract

$Mg_{1-x}Ni_xO$ ($0.43 \leq x \leq 0.53$) nanoparticles have been successfully synthesized via sol-gel methodology by using nitrates as the precursors of metal ions. We present the first report on the synthesis and antibacterial activity of $Mg_{1-x}Ni_xO$ nanoparticles below 100nm range. The effect of thermal treatment on the morphology, structure, composition, particle size, crystallite size and antibacterial activity of the nanoparticles has been explored by annealing at different temperatures i.e.; 500, 600 and 800°C. These studies have been carried out by using SEM, EDX and XRPD techniques. SEM results show that the nanomaterials have a spherical shape with average particle size range from 54-63nm Where, EDX spectra confirm the percentage composition of Ni, Mg and O in the nanoparticles. While XRPD has confirmed the face-centered cubic (FCC) geometry with NaCl-type structure with and negligible change in unit cell volume with variation in Ni contents. The crystallite size ranges from 10.8, 19.27 and 30.17nm and increases with increase in annealing temperature. Smallest particle and crystallite size along with higher oxygen and Mg contents led to strong antibacterial activity for the sample annealed at 500°C. Results of antibacterial activity show their possible utilization for water purification, hydrogels formation and packaging materials.

Key Words: $Mg_{1-x}Ni_xO$; Nanocomposite; Single Phase; Antibacterial; Water purification.

List of Figures

List of Tables

Abbreviations and symbols

MgO	Magnesium Oxide
NiO	Nickel Oxide
SEM	Scanning electron microscopy
XRPD	X-ray powder diffraction
EDX	Electron dispersive x-ray spectroscopy
NP	Nanoparticles
H	hours
Min	Minutes
EDX	Electron dispersive x-ray spectroscopy
SC	Single crystal
°C	Degree Celsius
at-%	Atomic percent
EPR	Electron paramagnetic resoanance
M	Molar
DI	Deionized
FCC	Face centered cubic
Conc.	Concentration
w/V	Weight/Volume
MRSA	Methicillin resistant staphylococcus aureus
E. coli	*Eschersheim* coli
WH plot	Williamsons Hall plot
TPF	Thermal power factor
+ve	Positive
-ve	Negative
Ctrl	Control
EMR	Electro magnetic radiation
FIB	Focused ion beam

SE	Secondary electrons
Std.	Standard
BSE	Back Scattered Electron
EPMA	Electron probe Micro-analyses

Chapter 1: Introduction

1.1. Nanoscience and nanotechnology

Nanoscience is a compound word consisting of two parts; "*nano*" and "*science*". The word nano is well understood as a prefix in nano-seconds, nano-ampere nanometer etc. with a value i.e. 10^{-09}. While, the science includes biology, chemistry, physics and electronics etc. Hence it can be deduced that study of any object in the regime of nanometers is called nano-science. Nanotechnology was originated from the Greek word which means DWARF and its concept was first introduced by famous American scientist Richard Feynman in his lecture "there is a plenty of room at the bottom" [1]. and it can be defined as "It is the manipulation of matter on an atomic and molecular level" [2]. Hence nano-technology includes the synthesis of nanomaterials which comprise nano-objects and nanoparticles [3].Nanomaterials have modified optical, electrical and magnetic properties due to the enhanced surface to volume ratio and the chemical reactivity as compared to their bulk counter parts. All these differences occur due to quantum confinement effects [4]. Nanomaterials can be synthesized generally by two approaches,

a.   *Top down approach.* In this approach, macrostructures are milled or etched to form nanostructured materials.

b.   *Bottom up approach.* In this approach, the nanomaterials got synthesized by self-assembly and chemical synthesis method.

The various synthetic methods reported for nanomaterials are summarized in Table 1.1.

Table 1.1. Synthetic routes for nanomaterials

Top-Down Procedures (Physical methods)	Bottom-Up Procedures (Chemical Methods)
Laser Ablation	Sol-Gel method
Chemical Vapor Deposition (CVD)	Spray pyrolysis
Ball milling	Thermolysis
Electro-Deposition	Micro Emulsion

Nanomaterials are in quest of attention because of their enormous applications in electronics, optoelectronics, cosmetics, health, medicines, pharmacy, biotechnology [5], industry [6] information & communication technologies, catalysis [7], agriculture and defense etc.

1.2. Nano-materials and their Classification

There is no clear-cut definition for the nanomaterials but overall it can be concluded that those materials having at-least one dimension less than 100nm are encompassed in nanomaterials. Most of them occur naturally e.g. lipoproteins, viruses and ferritin etc [8]. The synthetic nanomaterials are again of two types.

a.   Fullerenes

b.   Nano particles

According to the dimension, nanomaterials can be classified into three classes as shown in Figure 1.1.

1.2.1. 0-Dimensional Materials

The materials with size range ≤ 10nm are 0-D materials. The movement of electrons in 0-D materials is confined in all three dimensions. In these materials the free motion of electrons is inaccessible. For example, nanoparticles, quantum dots and nano shells.

1.2.2. 1-Dimensional Materials

In these materials, movement of electrons is confined to two dimensions and is free to move only along 1 dimension.Nanowires, nanorods and nanofibers are included in the examples.

1.2.3. 2-Dimensional Materials

In this type of materials, the electronic movement is confined only in one dimension and it is allowed in remaining two dimensions. For example, thin films and nano belts.

1.2.4. 3-Dimensional Materials

The materials, in which electrons are free to move in all dimensions and the movement of electrons is highly available because of their porosity. Certain types of nano structures and nano clusters are embedded in them due to which they show amazing properties.
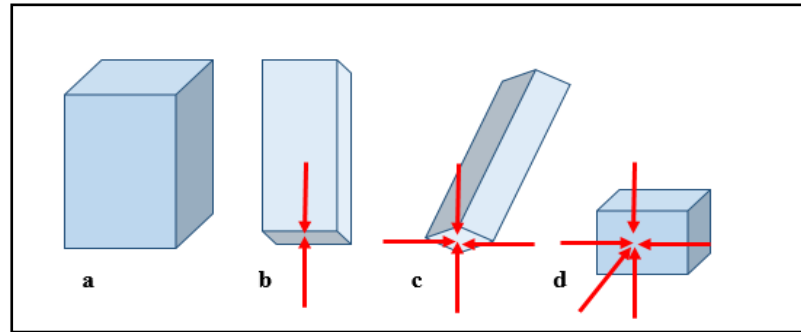
Figure 1.1. Dimension-based classification of nanomaterials

1.3.   Properties of nanomaterials

The properties of nanomaterials are usually different from their bulk counter parts and are highly dependent upon their grain size, shape and atomic compositions. Nanomaterials have the enhanced surface area and consequently high reactivity and the surface energy [4]. Different properties of nanomaterials are explained below.

1.3.1. Dimensional properties

Nanomaterials show quite different properties as compared to the bulk forms of the same materials. The reasons for this difference are; Surface to volume ratio and Quantum size effects.

a.   *Surface effects.* A well-known relation between surface to volume ratio and the size as given below,

Surface to volume ratio ∝ 1/size

As far as the size of a material is reduced, the number of dangling bonds increases which in turn increases the reactivity and other surface phenomena.

3

b.   *Quantum size effects.* In contrast to bulk materials the nanomaterials have discrete (quantized) energy levels instead of continuous energy levels due to extremely small size. This is due to the confinement of electronic wave function to the physical dimensions of the particles [4].

1.3.2. Optical properties

As the particle size reaches nanoscale the optical properties of the materials get changed from their bulk correspondents due to,

- Meager material effect
- Quantum confinement effect
- Surface plasmons
- Escalation of band energy
- Discrete band gaps formed (quantized levels)
- Formation of surface states

As the particle size changes from bulk to nano regime the metals can be converted to semiconductors and insulators due to the formation of band gaps, as shown in Figure 1.2. When nanomaterials interact with EM radiations they show blue shift. For example in the ZnS coated CdSe quantum dots blue shift appears as the size is reduced [9].
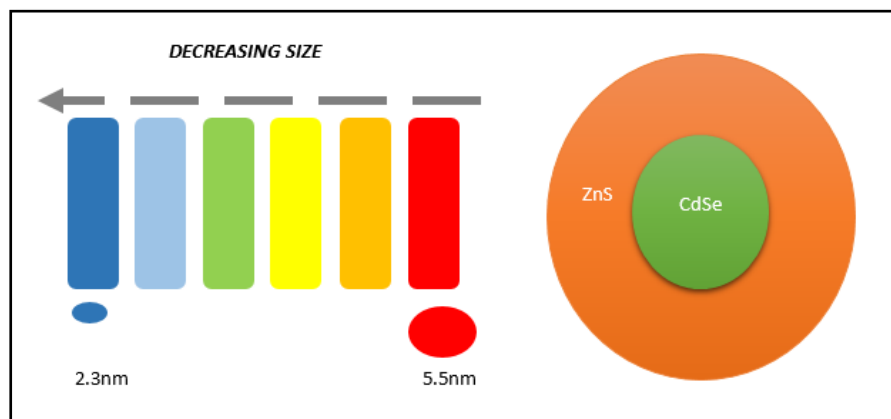
Figure 1.2. Appearance of blue shift due to reduction of size in CdSe quantum dots

1.3.3. Electrical properties

The electrical properties of nano-materials make them suitable for many technology applications [10]. Electrical properties are briefly described below.

- **Resistivity.** The reluctance to the flow of electrical current is called resistivity. It is measured in Ωm and mathematical expression is given below

$$\rho = R\frac{A}{l}$$

Where **R** is the *resistance,* **A** is the *cross-sectional area* and *l* is the *path length* of the material. Now a day the target is to synthesize the materials with the fewer value of the resistivity for the establishment of low-cost electronic devices. Daniel Huang et al synthesized the low resistance gold nanoparticles [11].

- **Conductivity**. The compatibility of a material for electrical current is called conductivity. Mathematically it can be expressed as follow,

$$\sigma = \frac{1}{\rho}$$

The gold nanoparticles show 70% enhanced conductivity as compared to the bulk [11]. The DC conductivity of NiO nanoparticles has been enhanced in order of six to eight times as compared to nickel oxide single crystal [12].

- **Dielectric strength**. The capability of a material to tolerate the applied voltage expressed in kV/cm. It is inversely proportional to sample thickness, operating temperature and applied frequency. Nickel oxide nanocrystals with 2-3nm size show elevated values of ε' and ε'' at fewer applied frequencies because of viable dielectric amplification. All this can be credited to an existence of covering of conducting grain boundaries over the insulating grains [12, 13].

- **Temperature coefficient of resistance**. The variation of resistance with a change of temperature is called temperature coefficient of resistance, measured in per °C. The resistance increases with increase in temperature for the metals, e.g., temperature coefficient for silicon is -0.007 per °C.

- **Thermoelectricity.** The materials which show thermoelectric effect are called thermoelectric materials. *Thermoelectricity* can be defined as the production of electric

voltage due to temperature difference and vice versa. The ability for thermoelectricity is measured by the figure of merit (zT).

$$zT = \frac{\propto^2 T}{\rho k}$$

Where $\propto$ is *Seebeck coefficient*, ρ is *electrical conductivity* and **k** is the *thermal conductivity*. The thermoelectric materials can be *p-type* and *n-type*. For example, Al-doped ZnO ($Al_{0.02}Zn_{0.98}O$) is an n-type thermoelectric material with zT=0.3 at 1000K [14].

1.4.   Applications of nanomaterials

Nanomaterials possess astonishing properties and show number of applications in various fields of chemistry, biology, electronics and physics etc. An overview of applications of nanomaterials is shown in Figure 1.3, due to the unique surface to volume ratio of nanomaterials, make them suitable every property of nanomaterials makes them suitable applicant for different fields.

Antibacterial	Batteries	Biomedicine	Photoelectronics
Displays	Tissue Engineering	Thermoelectrics	Sensors
Solar cells	Agriculture	Catalysis	Environment
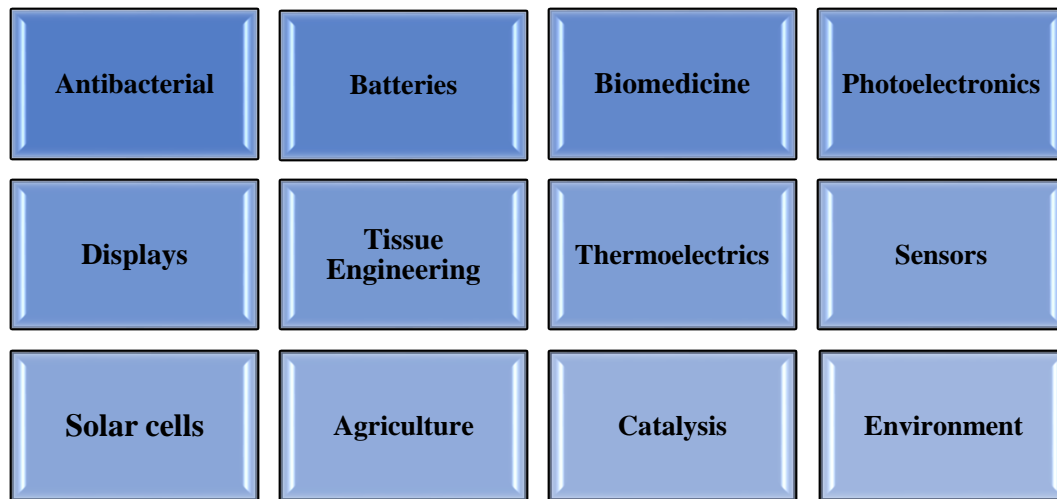
Figure 1.3. Applications of nanomaterials

For the catalytic application of nanomaterials a large surface area and a high number of dangling bonds are required in order to ensure the high reactivity. Many types of nanoparticles like Au, NiO and bimetallic Ni-Fe have been used in electro-oxidation of

methanol, thermal decomposition of ammonium perchlorate and hydrodechlorination of trichloroethylene to hydrocarbons respectively [15-19].

Similarly, nanomaterials have applications in biomedical, e.g. tissue engineering works with the aim of scaffolding the injured and smashed tissues by using nano-biotechnology. Many nanomaterials have promising properties for tissue regeneration and repairing. Nanotechnology has been applied to synthesize, handy and significant sensors that help to recognize the pollutants in the air, e.g., carbon nanotubes, SnO_2 nanowires and ZnO nanorods. Nanotechnology also plays an important role in the field of cosmetics, agriculture and environment. Where solar cells are the devices having an ability to convert light energy into an electric voltage by a physicochemical phenomenon i.e. photovoltaic effect. When a material enters a nano regime it leads to more stable, economical and tunable band gap solar cell. Most of the studies have been performed on silicon-based materials for the conversion of light signal to electrical signal [20-30].

The highest efficiency around 20% has been obtained by such materials, e.g.TiO_2 thin films can be easily synthesized by sol-gel, which is a potent material for this application and can also be used in dye-sensitized solar cells [31]. Nanomaterials have made it possible to create the portable, flexible and economical LEDs [32]. Many nanomaterials like NiO, PbTe, PbSe and silicon nanowires etc. are reported to be used in this application [33].

1.4.1. Antibacterial Materials

Bacterial pollution is present everywhere, like in atmosphere, water and land. Similarly, every utility .e.g. water, air, food, fabric, etc. each and everything is potent to bacterial pollution. So it is a need of the day to have an antibacterial agent for water treatment, as a disinfectant for food packaging as well as in textile industries. There are a number of organic compounds that have been used as antimicrobial agents like penicillin, cephalosporin or carbapenems which are modified natural products [34]. But organic antibacterial agents are expensive, less stable and toxic for living organisms other than bacteria. So scientists are switching towards the inorganic antibacterial agents due to their feasible synthesis and high stability under harsh conditions. Among different inorganic species MgO, NiO, CaO, ZnO and TiO_2 have been widely studied as antimicrobial agents

[35]. Inorganic nanomaterials are drawing attentions because nanoparticles can get inside the bacteria due to their small size and they show enhanced antibacterial activity due to higher surface area.

1.5. Characterization techniques

1.5.1. X-Ray Powder Diffraction

X-ray powder diffraction is a very famous technique employed for phase identification and calculation of crystal structure and crystallite size unit homogenized sample.

1.5.1.1. Principle of XRPD

Constructive interference of X-ray beam and a crystalline specimen is the core concept of X-ray diffraction technique. The constructive interference produced by the interaction of monochromatic X-ray beam and specimen must obey the *Bragg's law*.

Bragg's law

In this law three parameters are related to each other as

$$n\lambda = 2d\sin\theta$$

Where

λ__Wavelength of incident light.

θ__diffraction angle.

d__line spacing (Inter atomic distance).

The EMR gets diffracted from the sample at a certain angle according to the interatomic spacing of each material. These diffracted X-rays are then detected, refined and estimated. In powder X-ray diffraction the sample is randomly oriented so it is scanned in a range of 2θ angle and all possible orientations of diffracted radiations are recorded.
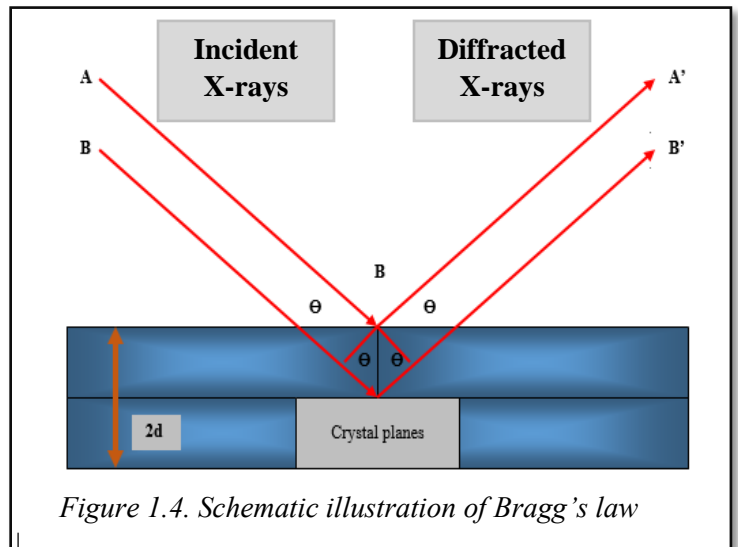
Figure 1.4. Schematic illustration of Bragg's law

1.5.1.2. Instrumentation of Powder XRD

The main components of the diffractometer are,

- X-ray tube
- Sample holder
- Detector

X-ray beam is produced by heating a filament in a cathode ray tube, then electrons are accelerated and directed to the targeted area by applying voltage the characteristic X-rays are produced. The X-ray generated by the targeted material (Mo, Cu, Fe, Cr) are collimated and oriented towards the sample. Finally detector records and processes the signal.

1.5.1.3. Sample preparation

To analyze the sample via XRPD three main components are required

- Material
- Material grinding instrument
- A sample holder

Figure 1.5. X-ray Powder Diffractometer

The steps for sample preparation are

- Few 10s mg of pure sample is taken.
- Placement of sample onto the sample holder. It can be either smeared onto a glass slide or packed into the sample container or can be sprinkled over a double sided sticky tape.
- Flat surface should be created.

1.5.1.4. Merits and demerits of XRPD Merits

Merits

- Forceful and quick technique.

- Mostly gives clear and explicit results.

- Requires a minimum amount of sample.

- XRPD data is easy to interpret.

Demerits

- To identify a new compound the sample must be the homogeneous & single phase.

- It requires the access to standardized reference file of all compounds.

- The sample is required in large quantity, i.e. 10's of a mg in powder form.

- The detection limit for mixed materials lies in the range of 2-5 %.

- It is too complicated to index the patterns for two non-isomeric crystals.

- High angle reflections get disturbed due to peak overlaying.

1.5.2. SEM (Scanning Electron Microscopy)

Scanning electron microscopy produces the image of the sample by using electron beam as a source. Its objective is to provide information regarding,

- Morphology

- Topography

- Phase distribution

- Compositional differences

- Presence and location of electrical defects

The superiority of SEM is because of,

- Formation of numerous signals

- Uncomplicated image generation phenomena

- Broad range of magnification (300 times of optical microscope)

- Attractive depth of field

- Resolution up-to 1nm

1.5.2.1. Working and Construction of SEM

The word "Scanning" means to focus the electronic beam onto the sample via an electromagnetic or electrostatic deflection and directing the emitting signal towards the monitor. The SEM uses a focused beam of high-energy electrons directed onto the sample via electric and magnetic fields. The similar trajectory and energy of incoming electrons are ensured by SEM optical column. As the high energy electronic beam falls on to sample placed on the specimen stage it can result in two types of interactions with the specimen,

a.   ***Elastic Collision.*** In this type of collision, the incoming electronic beam changes its path without loss of energy. As a result of this interaction, Back Scattered Electrons (BSE) are generated.

b.   ***Inelastic Collision.*** In this type of collision energy transformation from electronic beam to sample occurs. This results in the generation of Secondary Electrons (SE).

The electron guns are of three types:

- Tungsten Hexaboride thermionic electron gun

- Lanthanum Hexaboride thermionic electron gun

- The field emission gun

The SEM optical system consists of the condenser lens and an objective lens. The condenser lens is located below the electron gun and above the apertures. The main purpose of this lens is to reduce the diameter of the induced electronic beam. The second lens, i.e. objective lens in not different from the condenser lens as it reduces the diameter of coming probe in order to produce a "focused" image. The convergence or divergence of probe angle is determined by the objective lens aperture (probe forming aperture). The scan coils are located almost within the objective lens assembly. They are used to

- Regulate the beam position on the specimen

- Scan the beam for image production

11

- Decide the image magnification

- Fix a probe for X-ray analysis

A variety of detectors have been used in SEM, one of them is Everhart-Thornley (ET) Detector. It is used to observe the surface or morphology of the specimen. It is also known as SE detector as it collects the low energy secondary electrons. In the instrument, it can be placed within the sample chamber or within the optical column. The second type of detectors used in SEM is BSE detectors which respond to only high energy SE electrons.
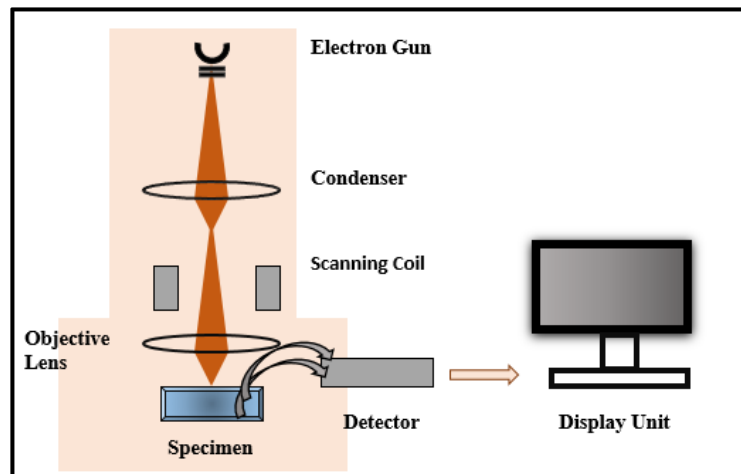
Figure 1.6. Assembly and working of SEM

1.5.2.2. Sample preparation

For SEM analysis the sample should meet some requirements prior to being mounted on the specimen stage,

A.   The surface of sample should be exposed
B.   It must be conductive
C.   It should be firmly attached to specimen mount

A   Methods for Exposing the Surface

a.   Fracturing. The cross section of a hard sample is prepared by fracturing. A crystalline material fractures along its cleavage plane in order to expose a flat cross section.

b.   Cutting. Ultra-microtome is used to cut the soft samples like polymers.

c. ***Mechanical Polishing.*** Many metals and minerals are mechanically polished by embedding in a resin. As a result of mechanical polishing, the rough abrasives are changed to fine abrasives and the sample is fabricated onto the glass slide.

d. ***Milling by Ion Beam.*** In recent years different types of ion beams have been used to expose the cross-sectional area of the sample. e.g. *Focused ion beam (FIB);* it provides the cross section with the potential accuracy of few hundred nanometers and the *Broad ion beam milling*; which uses broad Ar beam and provides a broad cross section but potential accuracy is lower as compared to FIB.

e. ***Contrast Enhancement.*** Many specimens with flat and smooth surfaces SE do not provide good contrast. There are certain techniques for the contrast enhancement like,

- ***Selective Etching.*** Irregularities are created on the surface of the sample by physical or chemical etching and secondary electrons are used to observe internal structure.

- ***Staining.*** In this technique, heavy metals like Ru and Os are stained over few regions of the polymer surface and BSE are used for compositional analysis.

B   Coating. For nonconductive samples, the surface is coated with thin film of metal so as to make the surface conductive. Ion sputter coating and vacuum evaporation are the common methods for the coating.

C   Mounting the Sample

a.   Bulk samples. Conductive double sided tape or conductive paste is used to place the bulk sample over the mount. The uniformly shaped specimen can be clutched to an exclusive sample holder.

b.   Powder and particles. Some samples are dusted or dispersed, in the case of dusting the powder is widely spread over the conductive paste or conductive tape while in the case of dispersion the sample is suspended in a dispersion media and is dropped over aluminum foil and is dried.

1.5.2.3. Interaction of electronic beam with specimen

As the electrons interact with the sample they get scattered into it. The scattering range depends upon the energy of electrons, atomic number and density of the constituent

elements. This interaction happens via two ways, i.e. elastic and inelastic collision as already has been defined in section 1.5.2.1. As a result of elastic collisions (*Back scattered electrons)* BSE are produced and inelastic collisions generate (*secondary electrons)* SE*, characteristic X-rays* and *auger electrons.* Figure 1.7 shows the schematic diagram of various types of signals generated as a result of electron interaction with a specimen.
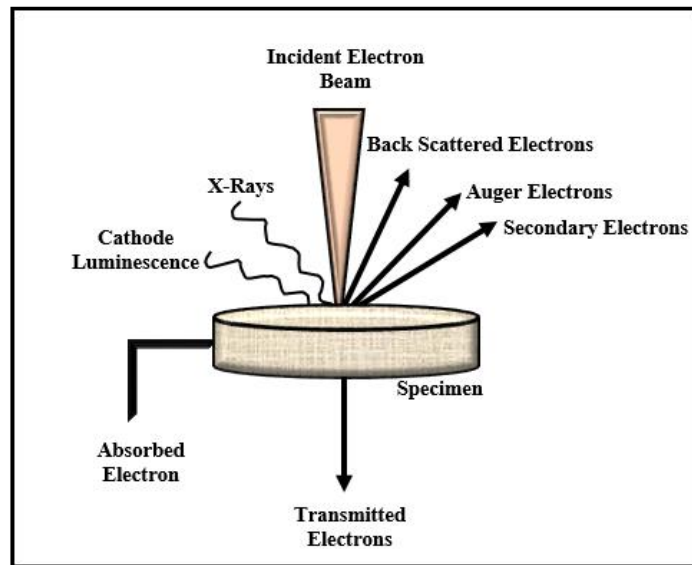
Figure 1.7. Emission of various types of electrons and EMR from sample

a.   Back scattered electrons (BSE)

The incident electron beam scatters back after interfering with the sample. The scattered electrons coming out of the sample at different trajectory are called BSE.

The beam energy and composition of the sample are the key factors for determining the depth from which BSE are escaped. These electrons possess more energy as compared to secondary electrons so they have greater sampling volume or the sample depth. The intensity of the BSE is the function of atomic number.

b.   Secondary electrons (SE)

When the electronic beam interacts with specimens the electrons from valence band are emitted and these are called secondary electrons. They are generated as a result of an inelastic collision and possess lower energy than back scattered electrons, i.e. 2-5 eV.

Due to lower energy, the SE generated from the deeper regions of an atom are absorbed suddenly. Only those electrons are emitted which are generated from the valence band. So they are very sensitive towards the surface. The sampling volume of SE is lower than BSE.

1.5.3. Energy Dispersive X-ray spectroscopy (EDX / EDS)

When electronic beam falls on the specimen it results in multiple interactions, i.e. elastic and inelastic interactions. The change in path and energy results in the volume interaction in the specimen. In addition to back scattered electrons and secondary electrons, the **characteristic X-rays** and **auger electrons** are also generated by inelastic collisions due to an emission of inner shell electrons. Both these processes compete with each other and both results into ionization of specimen. EDX is very useful for identification and compositional analysis of the specimen.
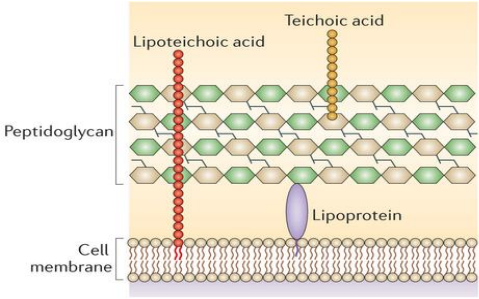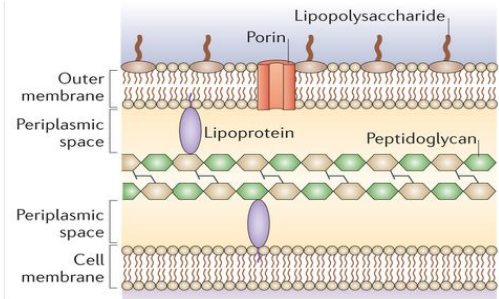
1.6.   Anti-Bacterial activity

Water is almost 71.4% of the total earth but only 3% of it is fresh water out of which only 0.015% is available to be used by humans because remaining is frozen water; glacier and ice [36].

An increase in urbanization and industrialization is the main causative agent to water pollution. It is a big challenge to get rid microbial water pollution. Many organic and inorganic antimicrobial agents in bulk form have been reported. Along with less efficiency there are other drawbacks like instability, needed in bigger quantities and the toxic effects for living beings. According to the review, most of the water available at consumer's end in Pakistan is beyond the WHO (World Health Organization) standards and about 20-40% of total diseases are due to an intake of contaminated water.[37]. Bacteria also cause various diseases like cholera, dysentery, hepatitis and typhoid etc. in humans, many diseases in animals like anthrax, calf necrotic diphtheria, septicemia etc., and in plants various types of problems like galls, wilting, leaf spotting, blights, rots, in addition to scabs and cankers. As far as morphology is concerned bacteria are unicellular, prokaryotic microorganism lacking a defined nucleus. Their mode of reproduction is simple binary fission. Broadly bacteria are classified as Gram +ve and Gram -ve bacteria depending

upon their cell wall compositions. Few important differences are mentioned in following Table 1.2.

Table 1.2. Differences between Gram-positive and Gram-negative bacteria

Gram-positive bacteria	Gram-negative bacteria
Bacteria which retains the color of gram stain even after the washing with acetone or alcohol.	They don't retain the color of gram stain.
They don't have an outer membrane.	They have an outer membrane.
Their wall is smooth with 20-30nm thickness.	Their cell wall is wavy and 8-12nm thick.
Their cell wall is composed of thick peptidoglycan and teichoic acid.	They have a thin layer of peptidoglycan with no teichoic acid.
They are susceptible to antibiotics.	They are resistant to antibiotics.
Methicillin Resistant *Staphylococcus Aureus* (MRSA)	*Escherichia coli* (*E. coli*)

1.6.1. Bacterial strains

In this project blow described bacterial strains have been used.

**a) Escherichia coli (*E. coli)*

Escherichia coli is a gram negative type of bacteria and the important and characteristics of this type have been already discussed in Table 1. 2. E. *coli* is usually known as fecal coliform bacteria and its presence in water indicates the poor sewage and sanitary system. It is present in small intestines of humans and animals. E. *coli* O157: H7 is one of the hazardous bacteria of this class [38]. That can cause swear cramps in intestines, bloody and non-bloody Diarrhea leading towards hemorrhaging and sometimes in children under 5 years its infection can lead toward hemolytic uremic syndrome. Those species which

produces shinga toxins can cause this syndrome. [39]. Humans can get this type of bacteria by intake of contaminated water and food.

b) Methicillin-Resistant Staphylococcus Aureus (MRSA)

It is a problem causing agent among both humans and the livestock. In cattle, bovine mastitis is very common among the infections caused by MRSA. In humans it can cause boils, inflammations, sores on the skin, infections in wounds etc. it can be transferred by simple "touch". It is usually difficult to treat with S. *aureus* so it is notorious as "super bug". It is categorized as an 'emerging infectious disease" (EIDs) [40].

1.6.2. Methods for antibacterial activity

There are various methods for the antibacterial activity test, i.e. colony count method, agar well method, agar diffusion method etc. But the most simple and feasible method for testing the antibacterial activity of inorganic nanoparticles is agar diffusion method or more precisely Disk Diffusion Method, this method is preferred because it is economic, feasible and easy to handle.

Agar Diffusion method. In this methodology the bacteria were grown on a media plate, i.e. agar plate and any wafer or disc containing antibiotic are placed over the media plate. After the incubation period "Zone of Inhibition" is measured. The strength of antibiotic is directly proportional to the diameter of the zone of inhibition.

Standardization. In the 1st step all the glass, Petri dishes and the media solution are autoclaved and then media is poured into the plates carefully in a nonpathogenic environment. The plates are incubated for 24h in order to check any type of contamination.

After incubation plates are inoculated with bacterial culture (grown in broth and diluted with saline solution) with the help of fire autoclaved spreader. Then the discs are immersed onto the media plate with the help of autoclaved forceps. After that plates are subjected to incubator already set at incubation temperature 37ºC.

1.7.   Aims and Motivation

The detailed literature survey led the attention to the synthesis of nanomaterials due to their applications in each and every field. Until now NiO and MgO have been synthesized in bulk form as well as in different nano-forms with many applications in the field of electronics, environment and biology.

There is a limited literature available for the synthesis of this composite in nanophase via wet chemical approach. There was a thirst to develop a feasible and economic wet chemical method for the synthesis of $Mg_{1-x}Ni_xO$ composite and to optimize the control of size, morphology and composition.

The main goals of the research work are given below,

➢ To develop a feasible and economic wet chemical synthesis methodology for single phase nanomaterial.
➢ To characterize the product.
➢ To check the potential applications of the material, especially antibacterial activity.

Chapter 2: Literature Survey

2.1. Nickel Oxide

Due to vast applications and diversity among transition metal oxides, *Nickel Oxide* is seeking attention both in bulk as well as nano regime. Among oxides of nickel NiO (1:1) is widely synthesized and well-characterized phase [7, 41, 42] but other phases like NiO_2, Ni_2O_3 are also claimed to exist but are not well studied [43]. Along with pure nickel oxide many composites and doped phases of nickel oxide have also been synthesized, e. g. $Ag_3Ni_2O_4$ [44], Ni-Al_2O_3 [45], $Ni_{0.1}Mg_{0.9}O$ [46].

2.2. Properties of Nickel Oxide (NiO)

2.2.1. Crystal Structure

Nickel (II) oxide has a *cubic* structure with NaCl-structure type, octahedral Ni^{2+} and O^{2-} sites shown in Figure 2.1.
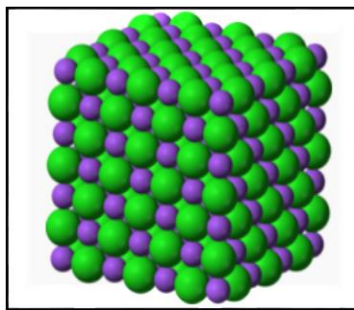
Figure 2.1. Cubic structure of NiO

Usually, NiO is in green color when Ni:O ratio is 1:1 as the ratio is disturbed NiO starts appearing black [47]. Crystallographic data of NiO collected from collected from X-ray single crystal [48] is summarized in Table 2. 1.

Table 2. 1. Crystallographic data of NiO [48]

Space group	$Fm\bar{3}m$ (225)
Lattice parameters	a =b = c = 4.1758 Å
Nickel atom coordinates	x= y = z= 0
Oxygen atom coordinates	x= y = z= 0.5

2.2.2. Antibacterial Property

The nanoparticles of NiO have been found effective against gram-positive bacteria [49]. The morphology of NiO nanomaterial has been found as an antibacterial activity directing parameter [50]. According to which nanotubes are stronger antibacterial agents as compared to nano-flowers.

2.2.3. Optical Property

The nickel oxide is a *p*-type semiconducting material [51]. The single crystal nickel oxide absorbs in the *red* region (λ= 708nm) at **1.75eV** and in *violet* (**2.75** and **2.95 eV**) and hence appears *green.* As the 1:1 ratio gets disturbed with an increase in oxygen content the absorption becomes stronger in visible region, as a result, the NiO starts appearing *black* [47]. As far as nanophase is concerned there is no notable red or blue shift in the band gap e.g. in the case of thin films (thickness ~ 60-180nm) NiO has a band gap value ~ **3.6 eV** which is comparable to the band gap of bulk NiO, i.e. **3.6 to 4 eV** [51]. NiO nanoparticles with 9nm diameter have a direct band gap of **3.56 eV** and according to electrochromic tests, these particles are promising material to be used as an electrode.[52]. Similarly, NiO nanowires equipped by electrodeposition method having diameter ~ 80nm show 3.74 eV band gap [53].

2.2.4. Electrical Property

Now a days the *ultra-capacitors* are seeking attentions due to their high power to meet the energy storage demands. They are also called *supercapacitors* with high power density and long cycle life [54]. Many transition metal oxides like Ru, Mn, Co and Ni oxides are the competent materials for this application. NiO particles synthesized via repeated immersion method shows improved electrochemical properties with an elevated capacitance of **455F/g** at a current of **10mA** [55].

2.2.5. Thermoelectric Property

Transition metal oxides have an immense number of electrical, mechanical and chemical properties but now a days they are also trending for *thermoelectric properties.* The extent of thermoelectricity is expressed by *Figure of Merit* (zT). Where zT is expressed as

$$zT = \frac{S^2 \sigma}{k}$$

Where,

S____Seebeck coefficient

σ____electrical conductivity

k____thermal conductivity [56].

NiO has been studied in this regard though NiO with stoichiometric ratio of 1:1 has extremely low value of electrical conductivity but it can be improved by increasing the vacancies in the structure of un-doped NiO [57]. For NiO $\sigma = 10^{-2}$S/m and S=101 µV/K has been reported [58]. S σ^2 known as *thermoelectric power factor* (TPF) is smaller for NiO due to electrical conductivity because it has band gap value around 3.4-4eV. But still it is an appealing material for energy harvesting and power generation because it's TPF has been enhanced by adding metallic dopants like Na and Li [59], [60].

2.3.   Applications of Nickel Oxide

Some important applications of NiO are summarized in Figure 2.2.
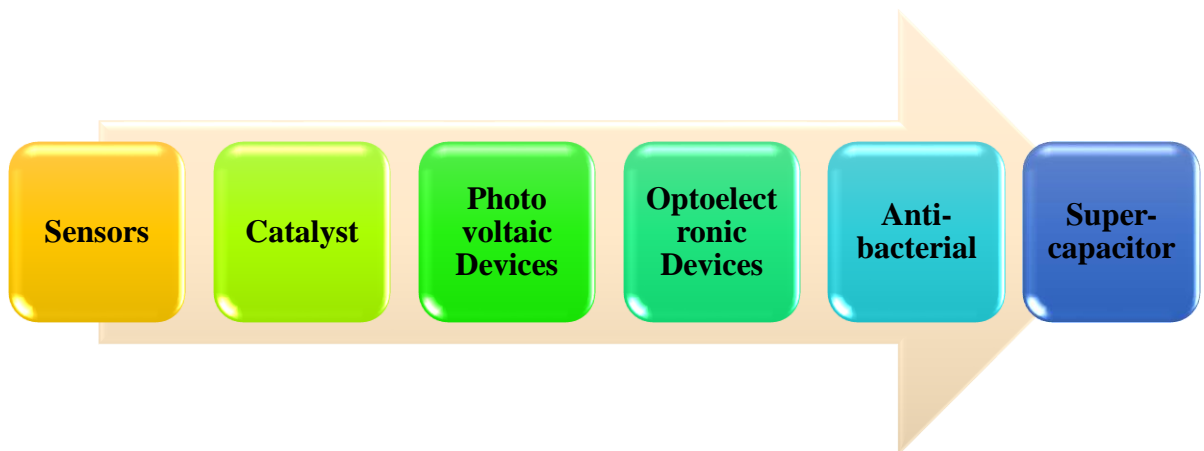
Figure 2.2. Applications of NiO

2.4. Properties of Magnesium Oxide

2.4.1. Crystal Structure

MgO has a rock salt type cubic geometry with crystallographic data [61] summarized in Table 2.2.

Table 2.2. Crystallographic data of MgO [61]

Space group	$Fm\overline{3}m$(225)
Lattice parameters	a = b = c = 4.217Å
Magnesium	x = y = z = 0
Oxygen	x = y = z = 0.5
Cell volume	75

2.4.2. Antibacterial activity

MgO nanomaterials have wide applications in water treatment because they can act as bactericide against both gram positive and gram negative bacteria. Due to the difference in cell membranes of gram-positive and gram-negative bacteria the 1st one can be more easily damaged. Because there is no outer membrane in gram positive bacteria and the cell wall is composed of layers of peptidoglycan instead of a complex structure present in gram negative bacteria [62, 63].

2.4.3. Optical properties

Magnesium oxide has acquired a lot of consideration due to its low heat capacity, high melting point [64] and in bulk form, it has 7.6 eV band gap. All these properties make it useful for insulation applications. MgO nanowires synthesized by using solvothermal method have reduced band gap energy to 4.51 eV[65]. Similarly, the MgO nanoparticles having average size ~ 16nm have 5.25 eV band gap energy. Even lower band gap has been reported for MgO nanowires, i.e. 3.54 eV[66]. Quantum size effect is responsible for this red shift in the band gap energy. Nanomaterials show absorption band at higher values (212nm) as compared to the bulk counterpart, i.e. 163nm. This effect can be credited to the low coordination of O^{2-} present at the surface [65].

2.4.4. Electrical property

There is a very limited literature regarding electrical properties of MgO. R. Mbarki et al have reported the electrical properties of MgO nanoparticles by using complex impedance spectroscopy. It was observed that resistance decreases with increase in temperature. Similarly, as the temperature is changed from 514 to 753°C the conductivity also changes from $4.2* 10^{-5}$ to $4.3*10^{-3}Sm^{-1}$. There is ionic conduction instead of hopping mechanism in the MgO nanoparticles [67].

2.5.   Applications of MgO

Applications of MgO can be summarized in Figure 2.3.
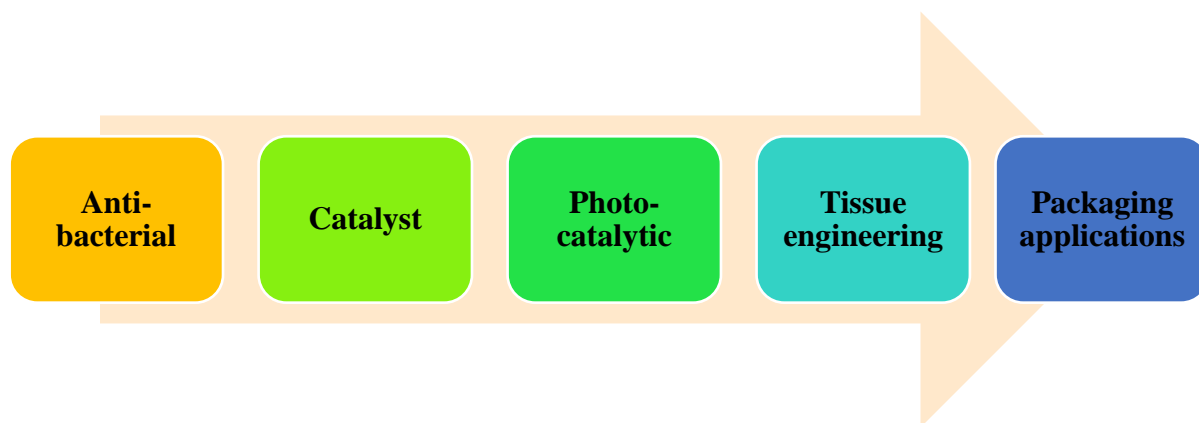
Figure 2.3. Applications of MgO nanoparticles

2.6.   Alkali metal oxide and transition metal composites

As bulk NiO and MgO have diverse properties and applications their doped nanocomposites have immense diversity and applications. In the nano nickel aluminate Al_2O_3/Ni have been used as catalysts, B/NiO nano-flowers are used as electrochemical capacitors. Similarly, there are a number of MgO nanocomposites with other elements like Zn/MgO and CaO/MgO nanocomposite having applications in photonic devices and photo-degradation respectively. Moreover, Ag/MgO nanocomposite has been reported for antibacterial activities [68-72].

23

2.6.1. Mg-Ni-O Nanocomposites

The fascinating properties of distinct NiO and MgO led some scientists to amalgamate their properties in a single ternary composite. Nickel magnesium oxide composite has been synthesized both in bulk [73] as well as in nano regime.

Mg-Ni-O composite in bulk form

The doping effect of different NiO percentages in SC (Single crystal) MgO on electrical conductivity was studied by Saxonberg et al. They have checked the effect of oxygen pressure from 10^{-1} to 10^{-7} atm on conductivity. The maximum electrical conductivity was observed from 10^{-4} to 10^{-3} atm. The result of maximum conductivity can be explained on basis of exchange between charge carriers. [73].

Later, $Ni_{0.1}Mg_{0.9}O$ was prepared by the thermal decomposition method of Ni and Mg bicarbonate at 800°C for 2h. The resultant product was subjected to BET technique, the results are summarized in Table 2.3 [46].

Table 2.3. Results of BET technique

Parameter	Value
Specific surface area of oxide	35 m2/g
Pore volume	0.345 cm3/g
Pore diameter	24.2nm

$Mg_xNi_{1-x}O$ (x is mole fraction of NiO and $0 \leq x \leq 1$) in form of solid solution was synthesized by decomposition of $Mg(OH)_2$ saturated with $Ni(NO_3)_2 \cdot 6H_2O$. It was observed that NO binding ability with Ni^{2+} is higher than Mg^{2+} when compared with pure MgO. This reactivity has been studied by using electron paramagnetic resonance (EPR) and density functional theory (DFT) [74].

Mg-Ni-O composite in nano form

Due to astonishing properties of this MgO-NiO solid solution in bulk, there is an interest in the synthesis of its nano-form. In this regard, Mg-Ni-O nanostructured solid solution was prepared by the combustion method by using Nickel and Magnesium nitrates and an organic fuel, i.e. urea. The particles obtained were uniform and size was in a range of 100-170nm [75]. Later on thin films of nickel magnesium oxide having the same atomic

composition as above were fabricated by a cheap method, i.e. spin coating by R.C. Boutwell et al. A colloidal solution has been prepared by adding magnesium and nickel acetate in 2-mothoxy ethanol and the covered suspension was stirred at 400 rpm for 1hr at 60°C. The solution was aged over 20h in order to get low-density gel, which was fabricated on quartz substrate via spin coater. The maximum thickness of the film was around 250nm [76]. Thin films of nickel magnesium oxide having the same atomic composition as above were again fabricated but by using radio frequency magnetron co-sputtering with NiO and MgO targets. The thickness of the deposited films was around 150-180nm. With an increase in Mg mole fraction from x =0 to 0.049 the band gap of $Ni_xMg_{1-x}O$ (x= 0.027 - 0.049) varies from 3.75 eV to 3.95 eV but the morphology of NiO wasn't changed due to a same crystal structure of MgO [77]. Mg-doped NiO thin films were also synthesized by using Ni and Mg chlorides as the precursors and by using spray pyrolysis technique. The band gap of the product varies from 3.56 to 3.62 eV with an increase in Mg concentration from 0 to 3% with the maximum thickness of the film was 100nm [78].

CHAPTER 3: Experimentation & Characterization Techniques

3.1. Experimental work

The experimental work includes; synthesis of Mg$_{1-x}$Ni$_x$O nanoparticles by sol-gel technique.

3.1.1. Sol-gel synthesis of NiMgO nanoparticles

Sol-gel method: It is a wet chemical technique and works via bottom-up route, i.e. synthesis of solid product from small molecules. The first stage is the formation of a stable colloidal solution (*sol*), in which hydrogen bonding and Vander Waal's forces are the main operative forces. The sol is converted to a three-dimensional integrated network which is called *gel* either by heating the *sol* or by the addition of the gelating agent. The *gel* is further placed for aging so that all the unreacted particles can get reacted. This method has advantages over other synthetic methodologies, it is a simple and an economical method.

Procedure

A very simple and feasible protocol was used for the synthesis of Mg$_{1-x}$Ni$_x$O nanomaterials. The list of the chemicals used in this protocol is mentioned in Table 3.1.

Table 3.1. List of chemicals used for synthesis of Mg$_{1-x}$Ni$_x$O nanoparticles

Sr. No	Chemicals	Chemical formula	Company	Purity (%)
1	Magnesium nitrate hexahydrate	$Mg(NO_3)_2.6H_2O$	Sima-Aldrich	99.99
2	Nickel nitrate hexahydrate	$Ni(NO_3)_2.6H_2O$	BDH chemicals Ltd Poole England	99.99
3	Sodium hydroxide	$NaOH$	Sigma-Aldrich	99.99
4	Ethylene glycol	$HO(CH_2)_2OH$	Merck-Millipore	99.99

First of all the 0.25M sol was prepared by adding nickel and magnesium nitrate precursors into ethylene glycol with continuous stirring at room temperature till the formation of a

clear solution. This sol was distributed into 4 parts, i.e. a, b, c and d. Four different aqueous concentrations of NaOH were prepared, i.e. 0.1, 0.5, 1 and 1.5M and added to these parts of the sol in the following order.

Table 3.2. The sol distribution with corresponding NaOH concentration

Sample code	NaOH conc.(M)
A	0.1
B	0.5
C	1
D	1.5

The addition of NaOH solution was carried out under constant stirring and sol was subsequently transformed into a green colored gel. Each gel was stirred for 10 minutes in order to achieve homogeneity. These gel samples were aged for 48 h by keeping static and subsequently washed with ethanol and water in order to remove unreacted nitrates. Later on washed gel was subjected to vacuum drying at 150°C for 3h and after grinding light green powder was subjected to annealing at 800°C for 3h which resulted into a grey colored powder. All samples were subjected to XRPD, SEM and EDX in order to optimize the NaOH concentration. The best results were obtained for the sample prepared by using 0.5M concentration. The optimized been employed to prepared the sample again but this time the dried gel was split into three parts and each part was annealed at 500, 600 and 800°C for 3h. The hierarchic diagram of the synthetic methodology is shown in Figure 3.1.
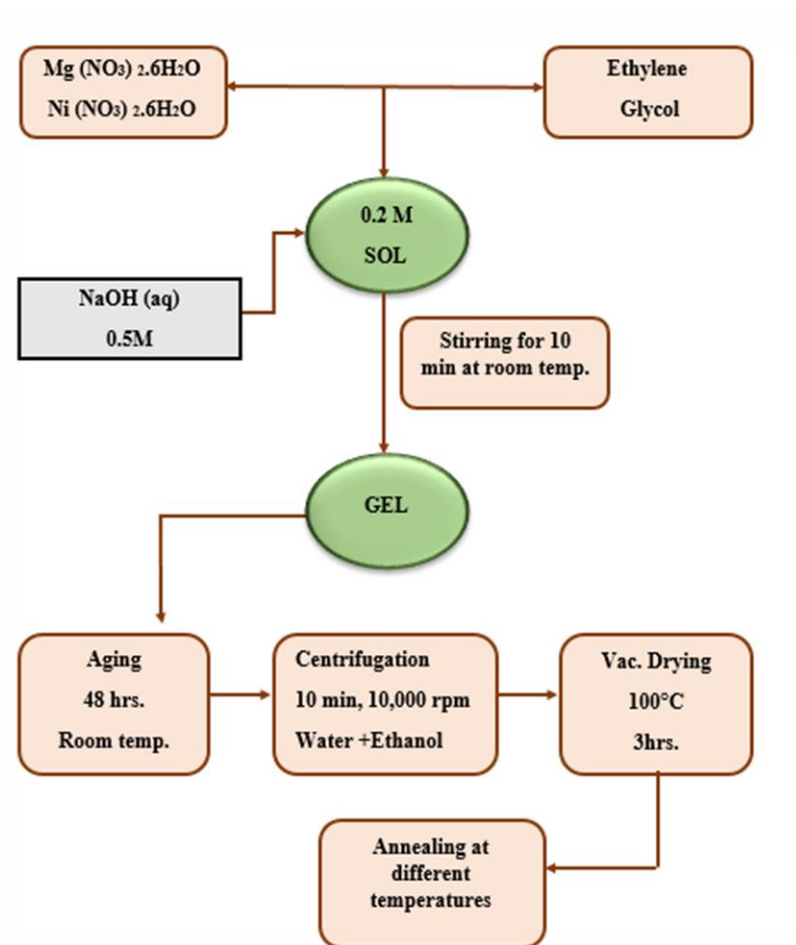
Figure 3.1. Hierarchic diagram of the synthetic methodology

3.1.2. Reaction Mechanism

In first the step when nitrates addition to the ethylene glycol leads to the formation of metal ions complexes with ethylene glycol as given in the following equation;

$$2Ni(NO_3)_2.6H_2O + HOCH_2CH_2OH \rightarrow Ni^{2+}(OCH_2CH_2O)^{2-} + 2HNO_3 + 6H_2O$$

$$2Mg(NO_3)_2.6H_2O + HO(CH_2)_2OH \rightarrow Mg^{2+}(OCH_2CH_2O)^{2-} + 2HNO_3 + 6H_2O$$
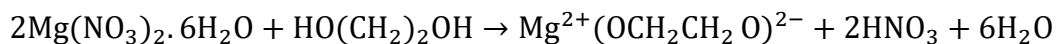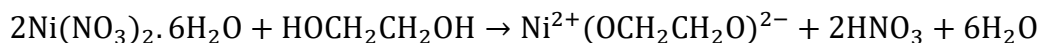
In the second step when gelating agent was added to the above reaction mixture respective metal hydroxides were formed as given in the following equation;

$$Ni^{2+}(OCH_2CH_2O)^{2-} + 2NaOH + 2HNO_3 \rightarrow Ni(OH)_2 + HOCH_2CH_2OH + 2NaNO_3$$

$$Mg^{2+}(OCH_2CH_2O)^{2-} + 2NaOH + 2HNO_3 \rightarrow Mg(OH)_2 + HOCH_2CH_2OH + 2NaNO_3$$
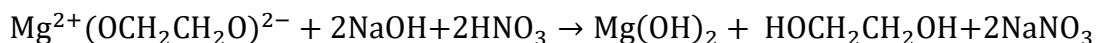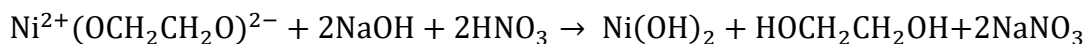
Both hydroxides coexist in the same reaction mixture (gel). Washing of gel led to the removal of ethylene glycol and nitrates. Remaining metal hydroxides were subjected to drying in order to obtain metal oxides.

$$Ni(OH)_2 + Mg(OH)_2 \xrightarrow{150°C} NiO + MgO$$
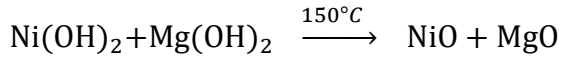
As a result of annealing at high temperature, both oxides were converted to a single phase ternary composite material, i.e. $Mg_{1-x}Ni_XO$

$$NiO + MgO \xrightarrow{(Annealing)} MgNiO$$
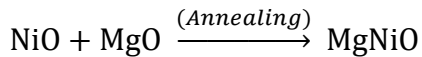
3.2.   Characterization

X-ray powder diffraction data were collected from each compound in as-cast and annealed state employing a Model STOE Germany operating at the 40kV operating voltage and 40mA current with monochromatic $Cuk_{\alpha 1}$ radiation in the range of (80°<2θ<100°). For qualitative analysis POWDER CELL program has been used [79] while quantitative Rietveld refinements of the X-ray powder diffraction data were performed with the FULLPROF program [80].

The drawback of this conventional *powder* method was that the diffraction peaks grossly overlap, thereby preventing the proper structure determination. *The "Rietveld Method" creates a virtual separation of these overlapping peaks*, thereby allowing the accurate determination of the structure. This *quantitative phase analysis* method has been so successful that nowadays the structure of materials, in the form of powders, are routinely being determined which are near to the accurate one [81]. The principle of Rietveld refinements is,

Calculated intensity at point i of the diagram

$$Y_{ic} = Y_{ib} + \sum_\emptyset S_\emptyset \sum_k G_\emptyset (2\theta_i - 2\theta_k) I_k$$

G__ normalized profile shape function

I___ intensity of the kth reflection

S___scale factor of phase ϕ Summation performed over all phases ϕ and over all reflections k contributing to the respective point.

y_{ib}__background

Intensity of Bragg reflections,

$$I_k = m_k L_k \; |F_k|^2 \; P_k \; A_k$$

Where,

m_k___multiplicity of kth reflection

L_k___Lorentz-polarization factor

$|F_k|^2$__structure factor

P_k___preferred orientation factor

A_k__absorption factor

The main goal is to minimize the residual function,

$$\sum_i w_i \, (Y_i^{obs} - Y_i^{cal})^2$$

Where,

$w_i = 1/y_i^{obs}$

y_i^{obs}___ observed intensity at the ith step

y_i^{calc}___ calculated intensity at the ith step

The as-cast and annealed powder samples were coated with graphite using standard procedures and scanning electron microscopy (SEM) via Electron Probe Micro-Analyses (EPMA) on an MIRA3 TESCAN equipped with an EDX system operated at 40 kV. The differences between measured and nominal compositions were found to be <1 at%.

3.3. Antibacterial Activity

Antibacterial activity of all the samples prepared at different temperature was studied against Gram-positive (MRSA) and Gram-negative (*E.coli*) bacteria. Co-amoxiclav was used as a positive control and simple filter paper disc dipped in distilled water was used as a negative control.

3.3.1. Materials and methods

Methodology. The Disc Diffusion method was selected for testing antibacterial activity of nanomaterial in which the sample is placed over plates in form of disc.

Broth. L.B Broth (yeast extract, sodium chloride, peptone, water) purchased from Merck. The culturing media for bacteria was prepared by adding 25g broth 1L distilled water. It was shaken and autoclaved to remove the impurities.

Saline preparation. Saline is the 9% solution of NaCl in distilled water, also autoclaved before use.

Preparation of bacteria. 10 ml of broth was added in two test tubes followed by the addition of bacterial strain in both test tubes. In 1st test tube DH5-alpha (*E.coli* strain) and in second test tube MRSA (Staphylococcus aureus strain) was added. And both were covered with foil and were placed for shaking at 37°C for 24h. After shaking the bacteria were diluted in the saline solution.

Growth media. Usually, nutrient agar is used as the growth medium for the bacteria during antibacterial activity measurements. 28g of the Nutrient agar purchased from OXOID was added into 100ml of Distilled water. The agar solution was autoclaved and mixed to get a homogenized solution.

Disc preparation. Discs with 6mm diameter were prepared with the help of a sterile puncher.

Sample preparation. The aqueous suspensions of the samples in four different weight percetage, i.e. 1%, 5%, 10% and 15 % were prepared.

Pouring. Autoclaved agar solution was poured into the autoclaved glass Petri dishes to maintain 5mm thickness. These agar plates were sealed and placed for incubation at 37 °C for 24h in order to check the contamination.

Plating. After removal from incubator, the contaminated plates were discarded and remaining plates were prepared to complete the experiment. The bacterial solution prepared in saline was spread by an autoclaved spreader over the agar plates. The discs of filter paper with 6mm diameter were immersed in relevant sample suspension and inserted

carefully onto the plate with the help of sterilized forceps. Separate forceps for each sample was used in order to avoid contaminations. The plates were sealed and placed for incubation at 37°C (98°F) for 24h.

Application of Control and standard. Co-amoxiclav was used as a standard and simple filter paper was used as a negative control The negative control was employed by using filter paper disc immersed with autoclaved distilled water. And standard was prepared by adding 1g Co-amoxiclav in 100 mL autoclaved distilled water.

Results collection. After incubation of prepared plates, the results were noted by measuring the inhibition zone including the disc with the help of scale. This test was carried out against both types of bacteria; gram positive (MRSA) and gram negative (*E. coli*) bacteria. The gram-negative bacteria are usually more resistant to the antibiotic and also more pathogenic as compared to gram positive bacteria.

CHAPTER 4: Results and Discussions

This chapter describes the results and discussion part on the synthesis, characterization and properties of $Mg_xNi_{1-x}O$ nanomaterial along with the findings of its antibacterial activity test.

4.1. Optimization of NaOH(aq) concentration

4.1.1. Crystallographic analysis

For the samples, prepared by using different molarities of NaOH showed that the best results were for the sample prepared with 0.5 M NaOH shown in Figure 4.1 which shows that the material is a single phase material. The crystallite size was calculated by using Scherrer formula that was 30.17nm.
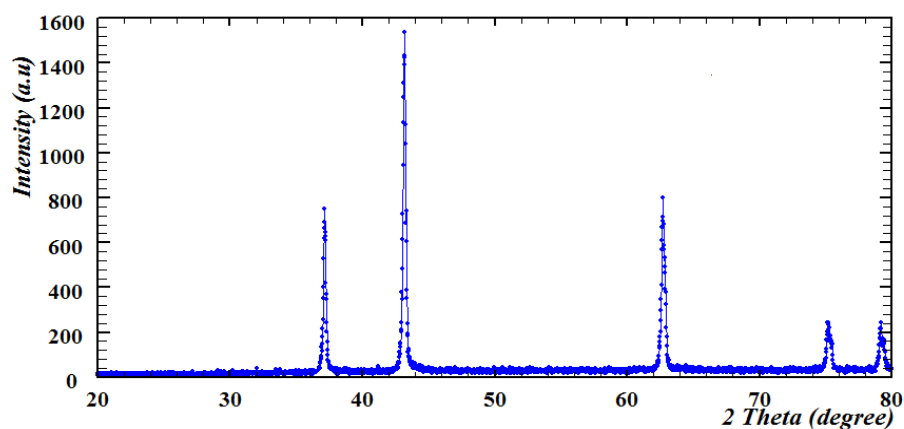
Figure 4.1. XRPD pattern of the sample prepared by using 0.5M NaOH(aq) solution, annealed at 800° C for 3h

4.1.2. Morphological and compositional analysis

In order to get results from SEM and EDX, aqueous dispersions of the prepared samples were prepared by 30 min ultra-sonication. The dispersions were then spread onto the glass slides in order to evaporate the solvent, after that samples were subjected to graphite coating with a sputter coater. These sputtered samples with conducting surface were subjected to Electron Probe Micro-Analyses (EPMA). First of all molarity of the gelating

agent, i.e. NaOH was optimized by using SEM, EDX and XRPD. Figure 4.2 shows the EDX and SEM of the samples prepared by using 0.1, 0.5, 1.0 and 1.5 M aqueous NaOH solutions and annealed at 800ºC for 3h, respectively.

For the 1st sample prepared by using 0.1 M NaOH shows good average particle size, i.e. 82nm but EDX results show that this contain only 3.6 at. % of Mg which is a non-reliable quantity. The best results were obtained with 0.5 M solution as it has the smallest average particle size, i.e. 65nm among all samples with sufficient amount of Mg (21.49 at. %). The samples prepared by 1.0 & 1.5M NaOH solutions have higher average particle size 84nm (19.97 at. % Mg) and 103.31nm (20.24 at. % Mg) respectively, as shown in Figure 4.5(c, c') and 4.5(d, d') and their relevant at-%age are summarized in Table 4.1. These observations led to the conclusion that 0.5 M gelating agent solution results in synthesis of monodispersed and uniform nanoparticles of NiMg oxide. Some extra peaks in EDX analysis are attributed to sample holder and the carbon from graphite coating, visible in Figure 4.1(a, b, c and d).

On the basis of these findings, the next experimental steps were carried out by using the optimized molarity that is, 0.5M NaOH, to prepare the materials in bigger quantities. This single phase sample was annealed at three different temperatures, i.e. 500, 600 and 800°C for 3h in order to see the thermal effect on morphology, composition and the structure.

Table. 4.1. at-%age of Ni, Mg and O obtained from EDX

Molarity	Mg (at-%)	Ni (at-%)	O (at-%)
0.1	3.67	47.97	48.37
0.5	21.49	27.70	50.81
1	19.97	24.72	53.31
1.5	20.24	24.89	54.87
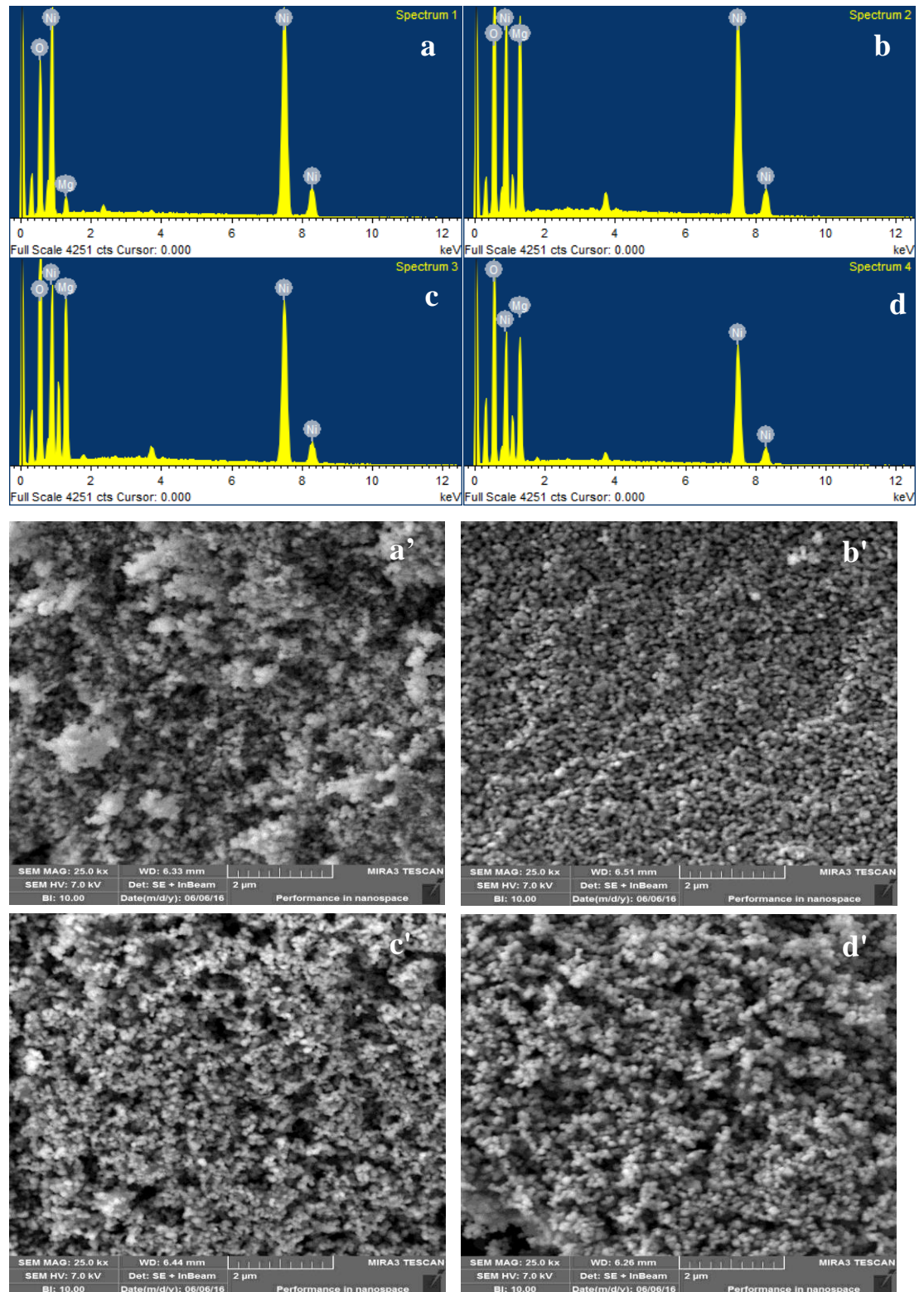
Figure. 4.2. EDX and SEM of samples prepared by using 0.1M (a, a'), 0.5M (b, b'), 1.0M (c, c') and 1.5M (d, d') NaOH solution and annealed at 800ºC for 3h

4.2.   Samples annealed at 500, 600 and 800°C

4.2.1. Crystallographic analysis

The remaining experiments were carried out by using these reaction conditions and three samples were prepared by annealing them at three different temperatures, i.e. 500°C, 600°C and 800°C and their XRPD patterns are shown in Figure 4.3.
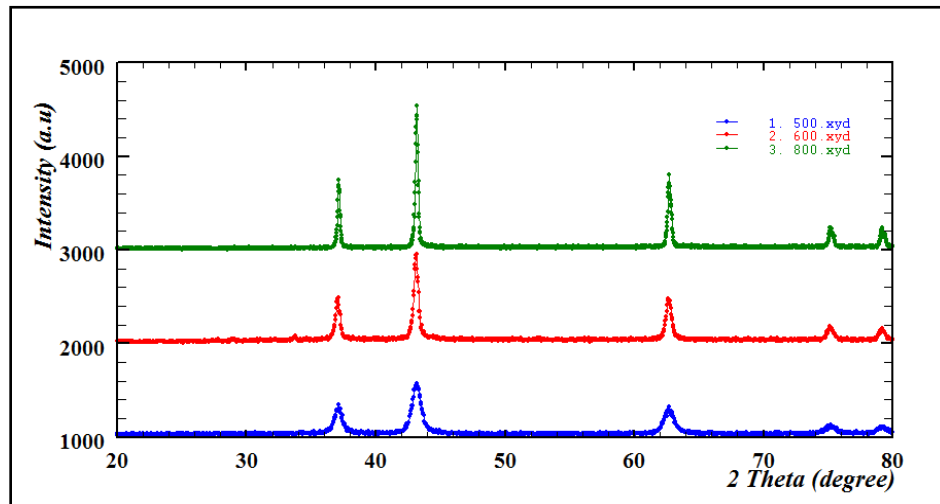
Figure 4.3. XRPD pattern of samples annealed at 500°C, 600°C and 800°C for 3h

4.2.2. Crystallite size

The XRPD patterns show that there is single phase material with (FCC) face centered cubic (space group $Fm\overline{3}m$; #225) symmetry after annealing at three different temperatures. At 500°C sample has very obvious peak broadening throughout the 2θ range while at the higher annealing temperature, an intensity of peaks increases due to increase in crystallinity and the peak broadening is obvious only at higher 2θ as shown in Figure 4.3. As far as the information regarding particle size from XRPD data is concerned usually these calculations are carried out by using the Scherrer equation [82] as given below,

$$D = \frac{K\lambda}{\beta Cos\theta}$$

Where

K_____shape coefficient

λ_____wavelength of incident radiation.

β_____full width half maxima (FWHM)

θ_____Bragg angle

The instrumental effects β factor also contribute to the peak broadening which is necessary to add or subtract from Scherrer results. According to Cullity the expression for correction of instrumental effects is [83] as given below,

$$\beta = \sqrt{\beta_{exp}^2 - \beta_{standard}^2}$$

β_{exp}_____β measured

$\beta_{standard}$_____β due to standard material

Another correction factor for Scherrer equation is the micro strain (ε) which contributes in broadening of diffraction peak.

$$\beta\varepsilon = 4\varepsilon\tan\theta$$

Williamson Hall (WH) plot is a simple way to separate the effects of micro strain and particle size on peak broadening. Following equation shows the contribution of particle size (D) and micro strain (ε) on the peak broadening with Lorentzian profiles,

$$\beta = \beta\varepsilon + \beta D$$

Here β is the summation of peak broadening due to micro strain and particle size. The WH plot is constructed by plotting sin θ against, $\beta Cos\theta/\lambda$, the resultant slope and intercept of the graph give the values of micro strain and particle size, respectively. The slope can be of three types and subsequently show three different results,

Positive slope___lattice expansion

Negative slope___lattice compression

Straight line____perfect crystal with no micro-strain

The data regarding particle size obtained by Scherrer equation and WH plot has been summarized in Table 4.2.

Table 4.2. Showing the Crystallite sizes, Strain (ε) and Particle sizes of $Mg_{1-x}Ni_xO$ $(0.43 \leq x \leq 0.53)$ *annealed at different temperatures.*

Temperature (°C)	2θ	*hkl*	*Crystallite size (nm)	**Strain ε (nm)	#Particle size (nm)
500	37.26	*(111)*	10.8	0.00122	54
600	37.18	*(111)*	19.27	0.00408	57
800	62.48	*(220)*	30.17	-0.00231	63

* Crystallite size values calculated by Debye Scherrer Formula at different *hkl.*
** Strain (ε) calculated from WH plots by using FWHM of all peaks in diffractrogram.
# Particle size values by SEM analysis

As it can be observed from the Table 4.2 that the strain values for all samples are too small to be neglected. The values of strain are positive for the samples annealed at 500 and 600°C showing minor lattice expansion while very small but negative value of strain for the sample annealed at 800°C shows a minor lattice compression.

4.2.3. Crystallographic parameters

The $Mg_xNi_{1-x}O$ nanocomposite has been prepared and annealed at three different temperatures, i.e. 500, 600 and 800°C for 3h. X-Ray powder diffraction data has been refined by employing Rietveld refinement via FullProf Suite.

The Summary of the refined parameters for the (500, 600 and 800°C) Magnesium Nickel Oxide is mentioned in Table 4.3. The values mentioned in the parenthesis shows the standard deviation along with the literature data of pure NiO and MgO [84, 85]. Rietveld refinements show the strong agreement between the measured and calculated XRD patterns which is clear from the amplitude of the blue line at the base as shown in Figure 4.4.
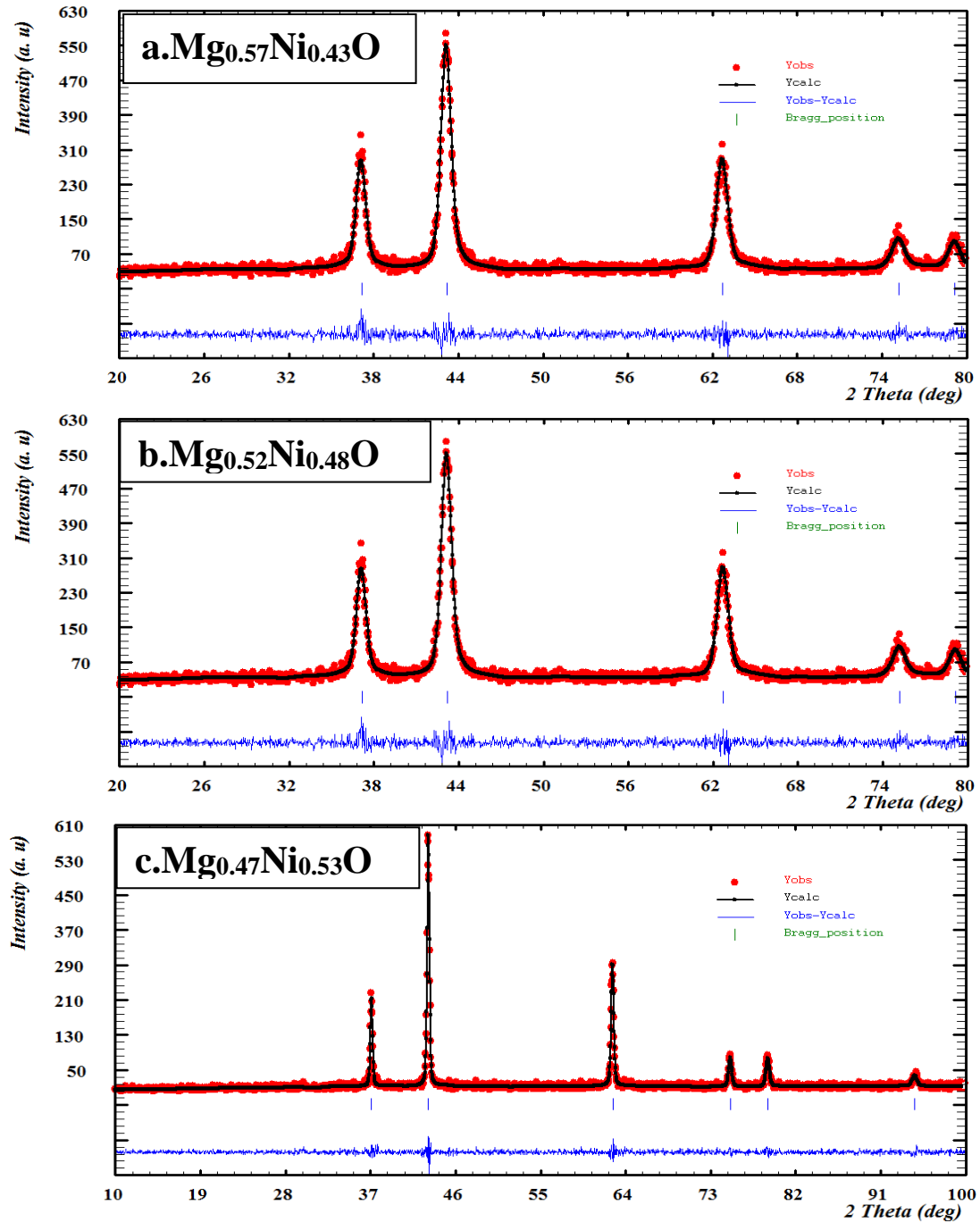
Figure 4.4. Rietveld refinements of XRPD results for the samples annealed at (a). 500, (b).600 and (c).800ºC

Table 4.3. Rietveld refinement results for Mg₁₋ₓNiₓO (0.43 ≤ x ≤0.53) {this work}nanomaterials in comparison to bulk literature all crystallized in space group $Fm\bar{3}m$; 225 with NaCl structure type

Parameters	Crystals data for (Mg $_x$ Ni$_{1-x}$)O XRPD nanoparticles {this work}			Bulk XRPD		
	500ºC	600 ºC	800 ºC	[86]	[87]	[88]
Formula from refinement	Mg$_{0.57}$Ni$_{0.43}$O	Mg$_{0.52}$Ni$_{0.48}$O	Mg$_{0.47}$Ni$_{0.53}$O	NiO	MgO	Mg$_{0.97}$Ni$_{0.03}$O
a (nm)	0.41856(1)	0.4176(5)	0.4007(8)	0.41795	0.4217	4.2115
M*(x=y=z=0) Occ.	0.57(9)+ 0.43(3)	0.52(3)+ 0.48(4)	0.47(3)+ 0.53(4)	1.00	1.00	0.97+0.03
U$_{iso}$	0.52(5)	0.23(13)	0.37(5)	-	-	-
O(x=y=z=0.5)Occ.	0.97(17)	1.00(2)	0.99(3)	1.00	1.00	1.00
U$_{iso}$	0.62(6)	0.74(2)	0.68(30)	-	-	-
V (Å^3)	73.29(4)	72.86(2)	64.33(3)	73	75	73.8
d (g/cm^3)	4.711	4.973	5.309	-	-	5.18
2θº	37.26	37.18	62.48	-	-	-
FWHM (º)	0.8013	0.4363	0.2770	-	-	-
R$_f$	1.45	1.85	3.34	-	-	-
R$_{bragg}$	2.73	3.48	5.35	-	-	-
χ^2	1.09	1.39	1.38	-	-	-
GOF	2.04	7.38	5.92	-	-	-

M* Mg+Ni

The variation in cell volume of Mg₁₋ₓNiₓO (0.43 ≤ x ≤0.53) Vs Ni concentration is plotted in Figure 4.5 which depicts the decreases with increase in Ni content because of its smaller ionic and crystallographic radii as compared to that of Mg.
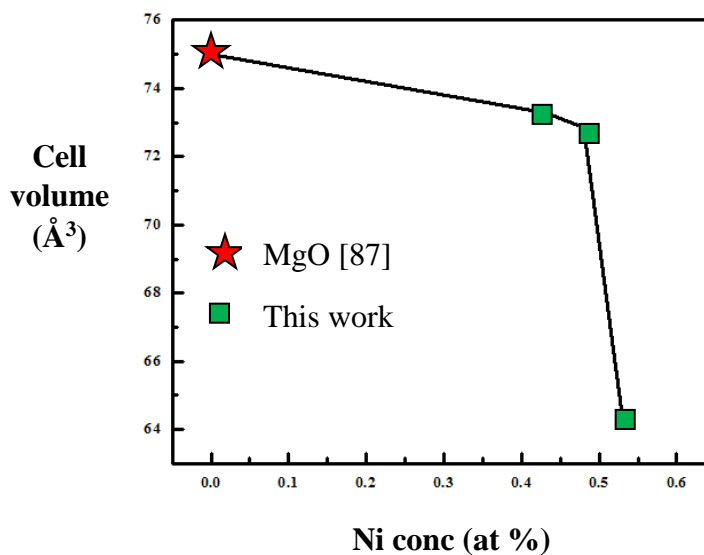
Figure 4.5.Change in cell volume Vs Ni content (at. %)

It can be observed from Figure 4.5 that with the increase in nickel content the cell volume is decreasing. The sample annealed at 800 ℃ contains highest Ni content and the lowest cell volume.

4.2.4. Morphological Analysis

On the basis of the findings descried in section 4. 1, the next experimental steps were carried out by using the optimized molarity that is,0.5M NaOH, to prepare the materials in bigger quantities. This single phase material was annealed at three different temperatures i.e. 500, 600 and 800℃ for 3h in order to see the thermal effect on morphology via SEM, These annealed samples retained morphology as nanoparticles but variation in size and oxygen contents have been observed. At 500℃ the average particle size is 54nm while at 600 and 800 ℃ material have 57 and 63nm average particle size, respectively. All samples were of dirty green color before annealing but after heat treatment at 600 and 800℃ they turned color to grey. The sample annealed at 500℃, which has so far smallest particle size and higher surface area, turned from dirty green to black because of the presence of high number of oxygen dangling bonds at the surface . This kind of color change with higher surface area and greater oxygen content is the reported property of NiO [48]. The pH analysis of 0.63g/L suspensions in DI water of all three materials reveals the values as 11.21, 10.84 and 10.73 for 500, 600 and 800 ℃, respectively. Higher oxygen contents in the sample annealed at 500℃ is obvious from it higher pH, as shown by bulk $Mg_{1-x}Ni_xO$ with higher oxygen contents [89]. The SEM results of these samples annealed at different temperatures are shown in Figure 4. 6.
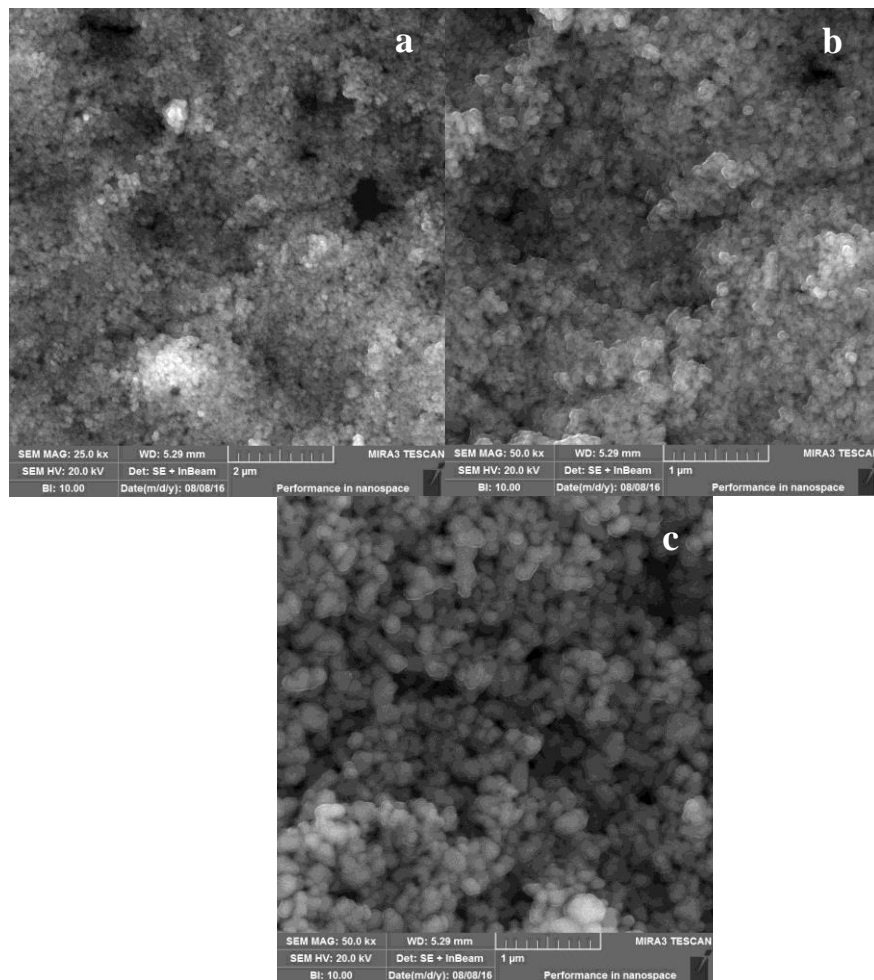
Figure 4.6. SEM results of samples annealed at (a) 500 (b) 600 (c) 800°C

4.3. Antibacterial activity of Mg$_{1-x}$Ni$_x$O (0.43 ≤ x ≤ 0.53) nanoparticles

Antibacterial activity of all the samples annealed at 500, 600 and 800°C has been evaluated against *E. coli* and MRSA strains by using Disk Diffusion method. Co-amoxiclav was used as standard and filter paper disks were used as negative control respectively. We have prepared three w/V (1, 5, 10 and 15%) aqueous suspensions for all the samples. The filter paper disks were used to employ the samples on bacterial cultures. The results of experiments on agar plates are shown in Figure 4.7.
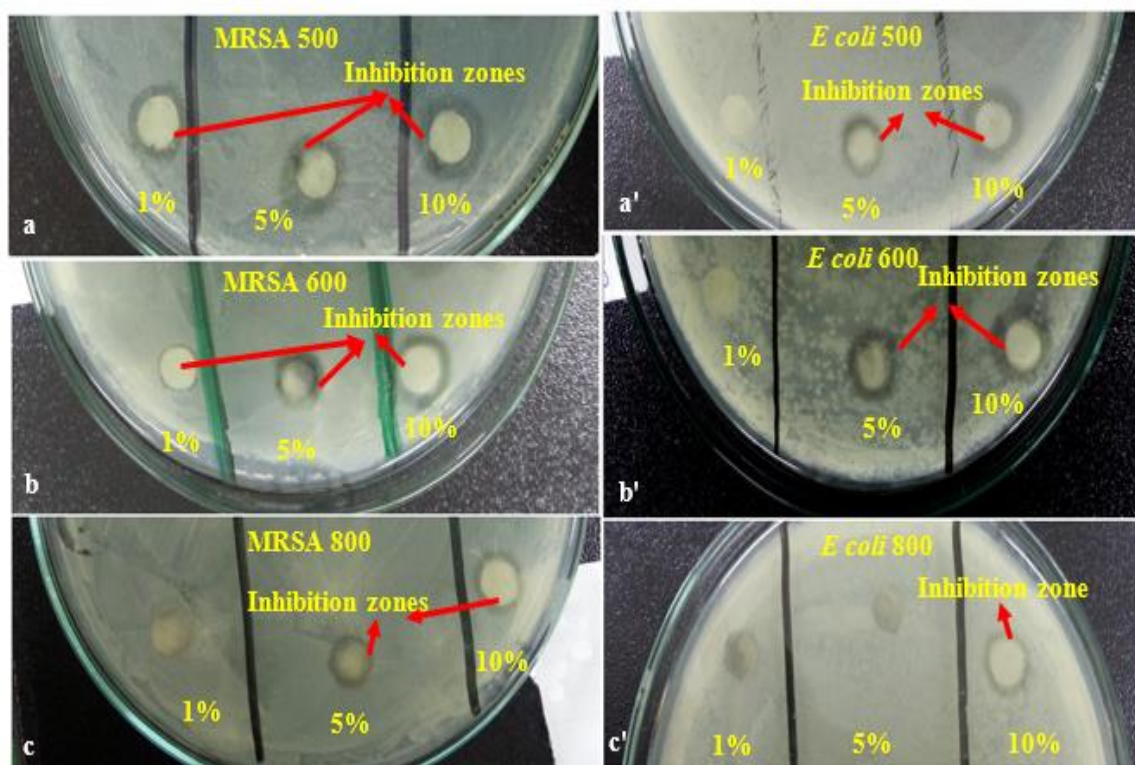
Figure 4.7. Antibacterial test plates for 500, 600 and 800 ºC sample against MRSA and E. coli bacterial strains

The diameter (including disk) inhibition zones are measured with the help of scale because the samples showed both types of inhibition, i.e. zone inhibition and contact inhibition. The average diameters of inhibition zones are mentioned in the Table 4.4. The bar charts have been plotted for all the tests by using these readings and are shown in Figure 4.8.

Table 4.4. Readings of inhibition zones (mm) from the agar plates

Strain	*Std.	**-ve ctrl	500°C			600°C			800°C		
			1%	5%	10%	1%	5%	10%	1%	5%	10%
MRSA I. Z[#](mm)	19	6	9	13	15	7	11	12.5	6	9	11
E coli I. Z[#](mm)	17	6	6	8	11	6	7	9	6	6	8

* Co amoxiclav used as standard
**Whatman Filter paper No.1 was used as a negative control
[#]Inhibition zone
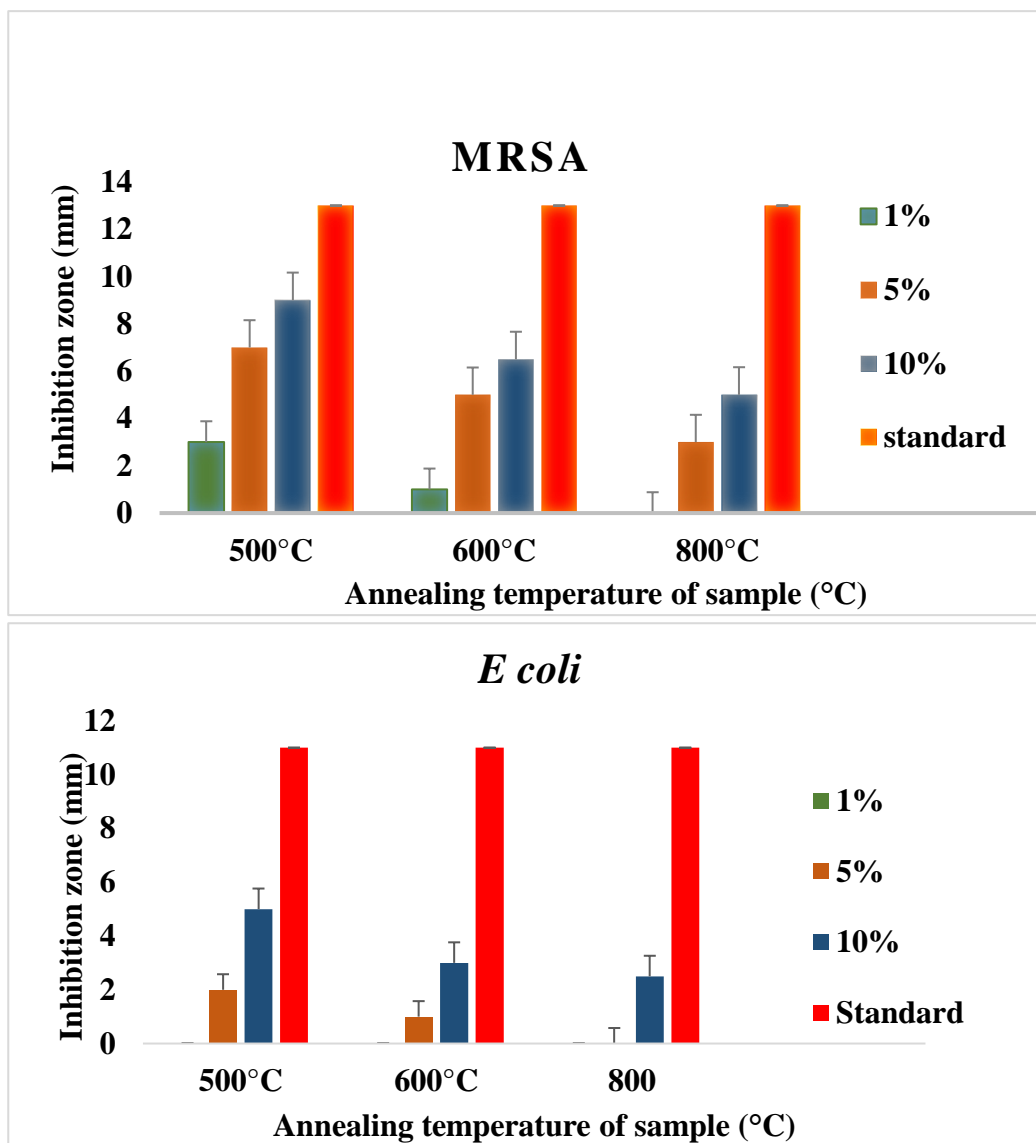
[Smaller the error bars, lesser will be the deviation in duplicate reading. All the error bars are small except for 5% concentrations used for *E. coli*. The reason behind this large error bar is the inactivity of 1% concentration].

Figure 4.8. Antibacterial activity of different concentrations, i.e. 1%, 5%, 10% and 15% (w/V) of $Mg_{1-x}Ni_xO$ ($0.43 \leq x \leq 0.53$) nanoparticles against (a) MRSA and (b) E.coli. The error bars indicate the standard error of mean

The red bars in the chart corresponds to co-amoxiclav (antibiotic) used as a standard. Maximum values for inhibition zone for both types of bacteria were obtained for the 10% suspension of the sample annealed at 500°C. Later, 15% suspension was also tested and it had almost same the results as for the 10% suspension. The smallest zones of inhibition

were obtained for suspensions of the sample annealed at 800°C. It doesn't show any zone with 1% and 5% suspension in case of *E. coli* but it gives 8mm zone with 10% suspension. In the case of MRSA, it showed inhibition zone of 9 and 11mm with 5% and 10% suspension, respectively. Test was repeated with its 15% suspension also but on average it gave similar results as that of 10% suspension. The suspensions of 600°C annealed sample show almost intermediate results between 500 and 800°C. The similar results with 10% and 15% can be either be attributed to the saturation point or as the maximum holding ability of the filter paper used to load the sample.

The mechanism behind the antibacterial activity of $Mg_{1-x}Ni_xO$ ($0.43 \leq x \leq 0.53$) nano-solid solution can be credited to the active O^{2-} generated from the surface of the nanomaterial and its stability. The availability of O^{2-} at the surface of nanomaterial controls the pH of its suspension in water. As it has been already reported that at lower pH values the self dismutation reaction proceeds and leads towards the generation of H_2O_2 which is also an antibacterial agent but its activity is lower than O^{2-}. This kind of combination of two O^{2-} ions with two H^+ ions liberates H_2O_2 and O_2 is also reported in case of NiO [89]. The highest antibacterial activity of the sample annealed at 500°C is attributed to smallest particle size which in turn has smallest crystallite size. Because of small size it is associated with the increased surface area which results in generation and stability of O^{2-} specie. The pH of these samples were measured and recorded, the highest value was found for the one annealed at 500°C with smallest particle and crystallite size and the least Ni contents.

Similarly, the results can also be related to elemental the composition of nanoparticles synthesized at different temperatures. As the annealing temperature was increased the Ni^{2+} content was increased in the nano solid solution. This increased occupancy of Ni^{2+} is mentioned in Table 4.3. Though this change is not too much but can it supports the results of reduced antibacterial activity for the sample prepared at 500, 600 and 800°C. The graphs shown in Figure 4.7 depict overall good antibacterial activity of the material against MRSA as compared to *E. coli*.

4.4. Conclusions and future aspects

The single phase, monodispersed $Mg_{1-x}Ni_xO$ ($0.43 \leq x \leq 0.53$) nanocomposite via simple, feasible and economical wet chemical method has been synthesized by optimizing the gelating agent contents. The effect of thermal treatment on morphology, structure, elemental composition and antibacterial activity has been studied. The results of SEM, EDX and XRPD depicted that particle and crystallite size of the nanomaterial increases with annealing temperature. The biggest particle size (63nm) and crystallite size (30.17nm) has been obtained for the sample annealed at 800°C. From antibacterial test we conclude that all samples strongly inhibit the growth of MRSA (gram +ve bacteria) as compared to *E. coli* (gram -ve bacteria). Moreover, the antibacterial activity is directly proportional to Mg content and it is inversely proportional to the crystallite and particle size. The best results have been observed for the sample annealed at 500ºC which has smallest crystallite and particle and highest surface area, oxygen and Mg content with 54nm and 10.8nm, particle and crystallite size, respectively. This sample also has the least Ni 0.43 at. % and highest Mg 0.57 at. % content. Another important factor controlling the antibacterial activity is the pH of the suspension. The best results were obtained for the sample with highest pH value, i.e. 11.21. The results of antibacterial test show its potential application for both types of bacteria, i.e. gram-positive and gra- negative. In future it will be tried to verify the antibacterial activity by using other methods of antibacterial activity and against other microbes like fungi. In future, the material can be utilized as an additive in packaging materials, hydrogels (wound dressing etc.) and water purification membranes.

References

[1]   N. Taniguchi, "On the Basic Concept of Nano-technology" Proceedings of the International Conference on Production Engineering, Tokyo, *Japan Society of Precision Engineering*, 1974.

[2]   K. E. Drexler, "Nanosystems: Molecular Machinery, Manufacturing and Computation," *John Wiley & Sons, Inc*, 1992.

[3]   V. Stone, B. Nowack, A. Baun, N. van den Brink, F. von der Kammer and M. Dusinska, "Nanomaterials for Environmental Studies: Classification, Reference Material Issues and Strategies for Physico-Chemical Characterisation," *Science of the Total Environment,* vol. 408, pp. 1745-1754, 2010.

[4]   E. Roduner, "Size Matters: Why Nanomaterials are Different," *Chemical Society Reviews,* vol. 35, pp. 583-592, 2006.

[5]   O. V. Salata, "Applications of Nanoparticles in Biology and Medicine," *Journal of nanobiotechnology,* vol. 2, p. 1, 2004.

[6]   M. Paradise and T. Goswami, "Carbon Nanotubes–Production and Industrial Applications," *Materials & Design,* vol. 28, pp. 1477-1489, 2007.

[7]   J. Park, E. Kang, S. U. Son, H. M. Park, M. K. Lee and J. Kim, "Monodisperse Nanoparticles of Ni and NiO: Synthesis, Characterization, Self-Assembled Superlattices and Catalytic Applications in the Suzuki Coupling Reaction," *Advanced Materials,* vol. 17, pp. 429-434, 2005.

[8]   D. P. Cormode, P. A. Jarzyna, W. J. Mulder and Z. A. Fayad, "Modified Natural Nanoparticles as Contrast Agents for Medical Imaging," *Advanced drug delivery reviews,* vol. 62, pp. 329-338, 2010.

[9]   B. O. Dabbousi, J. Rodriguez-Viejo, F. V. Mikulec, J. R. Heine, H. Mattoussi and R. Ober, "(CdSe) ZnS Core-Shell Quantum Dots: Synthesis and Characterization of a Size Series of Highly Luminescent Nanocrystallites," *The Journal of Physical Chemistry B,* vol. 101, pp. 9463-9475, 1997.

[10]   Q. H. Wang, K. Kalantar-Zadeh, A. Kis, J. N. Coleman and M. S. Strano, "Electronics and Optoelectronics of Two-Dimensional Transition Metal Dichalcogenides," *Nature nanotechnology,* vol. 7, pp. 699-712, 2012.

[11]   D. Huang, F. Liao, S. Molesa, D. Redinger and V. Subramanian, "Plastic-Compatible Low Resistance Printable Gold Nanoparticle Conductors for Flexible Electronics," *Journal of the electrochemical society,* vol. 150, pp. G412-G417, 2003.

[12]   V. Biju and M. A. Khadar, "Analysis of AC Electrical Properties of Nanocrystalline Nickel Oxide," *Materials Science and Engineering: A,* vol. 304, pp. 814-817, 2001.

[13]   V. Biju and M. A. Khadar, "DC Conductivity of Consolidated Nanoparticles of NiO," *Materials research bulletin,* vol. 36, pp. 21-33, 2001.

[14]   T. M. Tritt and M. Subramanian, "Thermoelectric Materials, Phenomena, and Applications: A Bird's Eye View," *MRS bulletin,* vol. 31, pp. 188-198, 2006.

[15]   M.-C. Daniel and D. Astruc, "Gold Nanoparticles: Assembly, Supramolecular Chemistry, Quantum-Size-Related Properties and Applications Toward Biology, Catalysis and Nanotechnology," *Chemical reviews,* vol. 104, pp. 293-346, 2004.

[16]   J. Luo, M. M. Maye, Y. Lou, L. Han, M. Hepel and C. J. Zhong, "Catalytic Activation of Core-Shell Assembled Gold Nanoparticles as Catalyst for Methanol Electrooxidation," *Catalysis today,* vol. 77, pp. 127-138, 2002.

[17]   B. Schrick, J. L. Blough, A. D. Jones and T. E. Mallouk, "Hydrodechlorination of Trichloroethylene to Hydrocarbons Using Bimetallic Nickel-Iron Nanoparticles," *Chemistry of Materials,* vol. 14, pp. 5140-5147, 2002.

[18]   Y. Wang, J. Zhu, X. Yang, L. Lu and X. Wang, "Preparation Of NiO Nanoparticles and their Catalytic Activity in the Thermal Decomposition of Ammonium Perchlorate," *Thermochimica Acta,* vol. 437, pp. 106-109, 2005.

[19]   Z.-Y. Zhou, N. Tian, J.-T. Li, I. Broadwell and S.-G. Sun, "Nanomaterials of High Surface Energy with Exceptional Properties in Catalysis and Energy Storage," *Chemical Society Reviews,* vol. 40, pp. 4167-4185, 2011.

[20]   H. Chen and R. Yada, "Nanotechnologies in Agriculture: New Tools for Sustainable Development," *Trends in Food Science & Technology,* vol. 22, pp. 585-594, 2011.

[21]   Y.-J. Choi, I.-S. Hwang, J.-G. Park, K. J. Choi, J.-H. Park and J.-H. Lee, "Novel Fabrication of an SnO_2 Nanowire Gas Sensor with High Sensitivity," *Nanotechnology,* vol. 19, p. 095508, 2008.

[22]   K. Fujihara, A. Kumar, R. Jose, S. Ramakrishna and S. Uchida, "Spray Deposition of Electrospun TiO$_2$ Nanorods for Dye-Sensitized Solar Cell," *Nanotechnology,* vol. 18, p. 365709, 2007.

[23]   A. Lohani, A. Verma, H. Joshi, N. Yadav and N. Karki, "Nanotechnology-Based Cosmeceuticals," *ISRN dermatology,* vol. 2014, 2014.

[24]   I. Mora-Seró, S. Giménez, T. Moehl, F. Fabregat-Santiago, T. Lana-Villareal and R. Gómez., "Factors Determining the Photovoltaic Performance of a CdSe Quantum Dot Sensitized Solar Cell: The Role of the Linker Molecule and of the Counter Electrode," *Nanotechnology,* vol. 19, p. 424007, 2008.

[25]   R. Nair, S. H. Varghese, B. G. Nair, T. Maekawa, Y. Yoshida and D. S. Kumar, "Nanoparticulate Material Delivery to Plants," *Plant science,* vol. 179, pp. 154-163, 2010.

[26]   J. J. Norman and T. A. Desai, "Methods for Fabrication of Nanoscale Topography for Tissue Engineering Scaffolds," *Annals of biomedical engineering,* vol. 34, pp. 89-101, 2006.

[27]   M. Stefaniuk, P. Oleszczuk and Y. S. Ok, "Review on Nano Zerovalent Iron (NZVI): From Synthesis to Environmental Applications," *Chemical Engineering Journal,* vol. 287, pp. 618-632, 2016.

[28]   J. Wang, X. Sun, Y. Yang, H. Huang Y. Lee and O. Tan*,* "Hydrothermally Grown Oriented ZnO Nanorod Arrays for Gas Sensing Applications," *Nanotechnology,* vol. 17, p. 4995, 2006.

[29]   L. Zhang and T. J. Webster, "Nanotechnology and Nanomaterials: Promises for Improved Tissue Regeneration," *Nano today,* vol. 4, pp. 66-80, 2009.

[30]   T. Zhang, S. Mubeen, N. V. Myung and M. A. Deshusses, "Recent Progress in Carbon Nanotube-Based Gas Sensors," *Nanotechnology,* vol. 19, p. 332001, 2008.

[31]   D. Kuang, J. Brillet, P. Chen, M. Takata, S. Uchida and H. Miura*,* "Application of Highly Ordered TiO$_2$ Nanotube Arrays in Flexible Dye-Sensitized Solar Cells," *ACS nano,* vol. 2, pp. 1113-1116, 2008.

[32]   L. Zhou, A. Wanga, S.-C. Wu, J. Sun, S. Park and T. N. Jackson, "All-Organic Active Matrix Flexible Display," *Applied Physics Letters,* vol. 88, p. 3502, 2006.

[33]   M. S. Dresselhaus, G. Chen, M. Y. Tang, R. Yang, H. Lee and D. Wang, "New Directions for Low-Dimensional Thermoelectric Materials," *Advanced Materials,* vol. 19, pp. 1043-1053, 2007.

[34]   F. von Nussbaum, M. Brands, B. Hinzen, S. Weigand and D. Häbich, "Antibacterial Natural Products in Medicinal Chemistry—Exodus or Revival?," *Angewandte Chemie International Edition,* vol. 45, pp. 5072-5129, 2006.

[35]   Z.-X. Tang and B.-F. Lv, "MgO Nanoparticles as Antibacterial Agent: Preparation and Activity," *Brazilian Journal of Chemical Engineering,* vol. 31, pp. 591-601, 2014.

[36]   T. Ahmed, A. Pervez, M. Mehtab and S. K. Sherwani, "Assessment of Drinking Water Quality and it's Potential Health Impacts in Academic Institutions of Abbottabad (Pakistan)," *Desalination and Water Treatment,* vol. 54, pp. 1819-1828, 2015.

[37]   F. Nabeela, A. Azizullah, R. Bibi, S. Uzma, W. Murad and S. K. Shakir*,* "Microbial contamination of drinking water in Pakistan—a review," *Environmental Science and Pollution Research,* vol. 21, pp. 13929-13942, 2014.

[38]   K. L. MacDonald, M. J. O'Leary, M. L. Cohen, P. Norris, J. G. Wells and E. Noll*,* "Escherichia Coli 0157: H7, an Emerging Gastrointestinal Pathogen: Results of A One-Year, Prospective, Population-Based Study," *Jama,* vol. 259, pp. 3567-3570, 1988.

[39]   D. A. Rasko, D. R. Webster, J. W. Sahl, A. Bashir, N. Boisen and F. Scheutz*,* "Origins of the E. Coli Strain Causing an Outbreak of Hemolytic–Uremic Syndrome in Germany," *New England Journal of Medicine,* vol. 365, pp. 709-717, 2011.

[40]   M. Hawkes, M. Barton, J. Conly, L. Nicolle, C. Barry and E. L. Ford-Jones, "Community-Associated MRSA: Superbug at our Doorstep," *Canadian Medical Association Journal,* vol. 176, pp. 54-56, 2007.

[41]   S. Chakrabarty and K. Chatterjee, "Synthesis and Characterization of Nano-Dimensional Nickelous Oxide (NiO) Semiconductor," 2009.

[42]   N. Srivastava and P. Srivastava, "Synthesis and Characterization of (Single-and Poly-) Crystalline NiO Nanorods by a Simple Chemical Route," *Physica E: Low-Dimensional Systems and Nanostructures,* vol. 42, pp. 2225-2230, 2010.

[43]   N. N. Greenwood and A. Earnshaw, "Chemistry of the Elements," 1984.

[44]   T. Sörgel and M. Jansen, "Ag $_3$ Ni $_2$ O $_4$—A New Stage-2 Intercalation Compound of 2H–AgNiO$_2$ and Physical Properties of 2H–AgNiO$_2$ Above Ambient Temperature," *Journal of Solid State Chemistry,* vol. 180, pp. 8-15, 2007.

[45]   Y.-S. Seo, Y.-S. Jung, W.-L. Yoon, I.-G. Jang and T.-W. Lee, "The Effect of Ni Content on a Highly Active Ni–Al$_2$ O$_3$ Catalyst Prepared by the Homogeneous Precipitation Method," *international journal of hydrogen energy,* vol. 36, pp. 94-102, 2011.

[46]   F. Gómez-Garcia, J. Gomez, J. Jiménez-Mateos, S. Vic, J. Fierro and M. Peña, "Mg-Ni-O Based OCM Catalyst Obtained by Carbonate Precursor Method," *Solid state ionics,* vol. 63, pp. 325-331, 1993.

[47]   R. Newman and R. Chrenko, "Optical Properties of Nickel Oxide," *Physical Review,* vol. 114, p. 1507, 1959.

[48]   L. Bartel and B. Morosin, "Exchange Striction in NiO," *Physical Review B,* vol. 3, p. 1039, 1971.

[49]   T. Kavitha and H. Yuvaraj, "A Facile Approach to the Synthesis of High-Quality NiO Nanorods: Electrochemical and Antibacterial Properties," *Journal of Materials Chemistry,* vol. 21, pp. 15686-15691, 2011.

[50]   H. Pang, Q. Lu, Y. Li and F. Gao, "Facile Synthesis of Nickel Oxide Nanotubes and their Antibacterial, Electrochemical and Magnetic Properties," *Chemical Communications,* pp. 7542-7544, 2009.

[51]   H. Sato, T. Minami, S. Takata and T. Yamada, "Transparent Conducting P-Type NiO Thin Films Prepared by Magnetron Sputtering," *Thin Solid Films,* vol. 236, pp. 27-31, 1993.

[52]   X. Wang, J. Song, L. Gao, J. Jin, H. Zheng and Z. Zhang, "Optical and Electrochemical Properties of Nanosized NiO via Thermal Decomposition of Nickel Oxalate Nanofibres," *Nanotechnology,* vol. 16, p. 37, 2004.

[53]   Y. Lin, T. Xie, B. Cheng, B. Geng and L. Zhang, "Ordered Nickel Oxide Nanowire Arrays and their Optical Absorption Properties," *Chemical Physics Letters,* vol. 380, pp. 521-525, 2003.

[54]   A. Pandolfo and A. Hollenkamp, "Carbon Properties and their Role in Supercapacitors," *Journal of Power Sources,* vol. 157, pp. 11-27, 2006.

[55] W. Guo, K. Hui and K. S. Hui, "High Conductivity Nickel Oxide Thin Films by a Facile Sol–Gel Method," *Materials Letters,* vol. 92, pp. 291-295, 2013.

[56] S. Walia, S. Balendhran, H. Nili, S. Zhuiykov, G. Rosengarten and Q. H. Wang, "Transition Metal Oxides–Thermoelectric Properties," *Progress in Materials Science,* vol. 58, pp. 1443-1489, 2013.

[57] M. D. Irwin, D. B. Buchholz, A. W. Hains, R. P. Chang and T. J. Marks, "p-Type Semiconducting Nickel Oxide as an Efficiency-Enhancing Anode Interfacial Layer in Polymer Bulk-Heterojunction Solar Cells," *Proceedings of the National Academy of Sciences,* vol. 105, pp. 2783-2787, 2008.

[58] P. Patil and L. Kadam, "Preparation and Characterization of Spray Pyrolyzed Nickel Oxide (NiO) Thin Films," *Applied surface science,* vol. 199, pp. 211-221, 2002.

[59] W. Shin and N. Murayama, "Li-Doped Nickel Oxide as a Thermoelectric Material," *Japanese Journal of Applied Physics,* vol. 38, p. L1336, 1999.

[60] M. Dutt, R. Banerjee and A. Barua, "Transport Properties of Lithium and Sodium Doped Nickel Oxide," *Physica Status Solidi (a),* vol. 65, pp. 365-370, 1981.

[61] S. Sasaki, K. Fujino and Y. Takéuchi, "X-ray Determination of Electron-Density Distributions in Oxides, MgO, MnO, CoO and NiO, and Atomic Scattering Factors of their Constituent Atoms," *Proceedings of the Japan Academy. Ser. B: Physical and Biological Sciences,* vol. 55, pp. 43-48, 1979.

[62] S. Makhluf, R. Dror, Y. Nitzan, Y. Abramovich, R. Jelinek and A. Gedanken, "Microwave-Assisted Synthesis of Nanocrystalline MgO and its Use as a Bacteriocide," *Advanced Functional Materials,* vol. 15, pp. 1708-1715, 2005.

[63] M. Bindhu, M. Umadevi, M. K. Micheal, M. V. Arasu and N. A. Al-Dhabi, "Structural, Morphological and Optical Properties of MgO Nanoparticles for Antibacterial Applications," *Materials Letters,* vol. 166, pp. 19-22, 2016.

[64] M.-C. Wu, J. S. Corneille, C. A. Estrada, J.-W. He and D. W. Goodman, "Synthesis and Characterization of Ultra-Thin MgO Films on Mo (100)," *Chemical Physics Letters,* vol. 182, pp. 472-478, 1991.

[65] N. Hadia and H. A. H. Mohamed, "Characteristics and Optical Properties of MgO Nanowires Synthesized by Solvothermal Method," *Materials Science in Semiconductor Processing,* vol. 29, pp. 238-244, 2015.

[66]   A. A. Al-Ghamdi, F. Al-Hazmi, F. Alnowaiser, R. M. Al-Tuwirqi, Al-Ghamdi and
         O. A. Alhartomy, "A New Facile Synthesis of Ultra Fine Magnesium Oxide
         Nanowires and Optical Properties," *Journal of Electroceramics,* vol. 29, pp. 198-
         203, 2012.

[67]   R. Mbarki, A. Mnif and A. Hamzaoui, "Structural, Dielectric Relaxation and
         Electrical Conductivity Behavior in MgO Powders Synthesized by Sol–Gel,"
         Materials Science in Semiconductor Processing, vol. 29, pp. 300-306, 2015.

[68]   S. Chawla, K. Jayanthi, H. Chander, D. Haranath, S. Halder and M. Kar,
         "Synthesis and Optical Properties of ZnO/MgO Nanocomposite," *Journal of
         Alloys and Compounds,* vol. 459, pp. 457-460, 2008.

[69]   J. Lu, L. Gao, J. Sun, L. Gui and J. Guo, "Effect Of Nickel Content On The
         Sintering Behavior, Mechanical and Dielectric Properties of Al_2O_3/Ni Composites
         from Coated Powders," *Materials Science and Engineering: A,* vol. 293, pp. 223-
         228, 2000.

[70]   M. Shahid, M. A. Farrukh, A. A. Umar and M. Khaleeq-ur-Rahman, "Solvent
         Controlled Synthesis of CaO-MgO Nanocomposites and their Application in the
         Photodegradation of Organic Pollutants of Industrial Waste," *Russian Journal of
         Physical Chemistry A,* vol. 88, pp. 836-844, 2014.

[71]   J.-H. Yang, Q. Yu, Y. Li, L. Mao and D. Ma, "Batch Fabrication of Mesoporous
         Boron-Doped Nickel Oxide Nanoflowers for Electrochemical Capacitors,"
         Materials Research Bulletin, vol. 59, pp. 382-386, 2014.

[72]   X. Zhu, D. Wu, W. Wang, F. Tan, P. K. Wong and X. Wang, "Highly Effective
         Antibacterial Activity and Synergistic Effect of Ag-MgO Nanocomposite Against
         Escherichia coli," *Journal of Alloys and Compounds,* 2016.

[73]   J. S. Choi, H. Y. Lee and K. H. Kim, "Electrical Conductivity of Nickel Oxide-
         Magnesium Oxide Single Crystals," *The Journal of Physical Chemistry,* vol. 77,
         pp. 2430-2433, 1973.

[74]   M. Chiesa, M. C. Paganini, E. Giamello, C. Di Valentin and G. Pacchioni,
         "Bonding of NO on $Ni_xMg_{1-x}O$ powders: an EPR and Computational Study,"
         Journal of Molecular Catalysis A: Chemical, vol. 204, pp. 779-786, 2003.

[75]   K. V. Rao and C. Sunandana, "XRD, Microstructural and EPR Susceptibility Characterization Of Combustion Synthesized Nanoscale $Mg_{1-x}Ni_xO$ Solid Solutions," *Journal of Physics and Chemistry of Solids,* vol. 69, pp. 87-96, 2008.

[76]   R. Boutwell, M. Wei, A. Scheurer, J. Mares and W. Schoenfeld, "Optical and Structural Properties of NiMgO Thin Films Formed by Sol–Gel Spin Coating," *Thin Solid Films,* vol. 520, pp. 4302-4304, 2012.

[77]   Y. H. Kwon, S. H. Chun and H. K. Cho, "Controllable Band-Gap Engineering of the Ternary $Mg_x Ni_{1-x}O$ Thin Films Deposited by Radio Frequency Magnetron Sputtering for Deep Ultra-Violet Optical Devices," *Thin Solid Films,* vol. 529, pp. 417-420, 2013.

[78]   M. B. Amor, A. Boukhachem, K. Boubaker and M. Amlouk, "Structural, Optical and Electrical Studies on Mg-Doped NiO Thin Films For Sensitivity Applications," *Materials Science in Semiconductor Processing,* vol. 27, pp. 994-1006, 2014.

[79]   W. Kraus and G. Nolze, "POWDER CELL–A Program for the Representation and Manipulation of Crystal Structures and Calculation of the Resulting X-Ray Powder Patterns," *Journal of Applied Crystallography,* vol. 29, pp. 301-303, 1996.

[80]   T. Roisnel and J. Rodríquez-Carvajal, "WinPLOTR: A Windows Tool for Powder Diffraction Pattern Analysis," in *Materials Science Forum*, 2001, pp. 118-123.

[81]   H. Rietveld, "A Profile Refinement Method for Nuclear and Magnetic Structures," *Journal of Applied Crystallography,* vol. 2, pp. 65-71, 1969.

[82]   L. V. Azároff and M. J. Buerger, The Powder Method*: In X-ray Crystallography*: McGraw-Hill, 1958.

[83]   M. Ganguly, S. Rout, H. Park, C. Ahn and I. Kim, "Structural, Dielectric and Optical Characterization of Cerium Doped Barium Titanate," *Phys Express,* vol. 3, pp. 1-12, 2013.

[84]   Z. Feng, V. S. Babu, J. Zhao and M. S. Seehra, "Effect of Magnetic Dilution on Magnetic Ordering in $Ni_P Mg_{1-P}O$," *Journal of Applied Physics,* vol. 70, pp. 6161-6163, 1991.

[85]   H. Vincent, M. Audier, S. Pignard, G. Dezanneau and J. Senateur, "Crystal Structure Transformations of a Magnetoresistive $La_{0.8}MnO_{3-\delta}$ Thin Film," *Journal of Solid State Chemistry,* vol. 164, pp. 177-187, 2002.

[86]   Z. Feng and M. S. Seehra, "Phase Diagram and Magnetic Properties of the Diluted FCC System $Ni_P Mg_{1-P} O$," *Physical Review B,* vol. 45, p. 2184, 1992.

[87]   H. Vincent, M. Audier, S. Pignard, G. Dezanneau and J. Senateur, "Crystal Structure Transformations of a Magnetoresistive $La_{0.8}MnO_{3-\delta}$ Thin Film," *Journal of Solid State Chemistry,* vol. 164, pp. 177-187, 2002.

[88]   Z. Feng, V. S. Babu, J. Zhao and M. S. Seehra, "Effect of Magnetic Dilution on Magnetic Ordering in $Ni_p Mg_{1-p} O$," *Journal of Applied Physics,* vol. 70, pp. 6161-6163, 1991.

[89]   T. Ohira and O. Yamamoto, "Effective Factor on Antibacterial Characteristics of $Mg_{1-X} Ni_X O$ Solid Solution," *Chemical Engineering Research and Design,* vol. 91, pp. 1055-1062, 2013.